Spiral Structure and Mass Inflows Barred-Spiral Galaxies

The Lin-Shu Symposium@Beijing
June 27, 2013

Woong-Tae Kim
Yonghwi Kim
Woo-Young Seo

Seoul National University
Korea

Outline

- Bar regions
  - Substructure formation
  - Location of nuclear rings
  - Longevity of dust lanes and ring star formation
- Spiral-arm regions
  - Extent and shape of gaseous arms
  - Gas inflows/outflows driven by spiral arms.

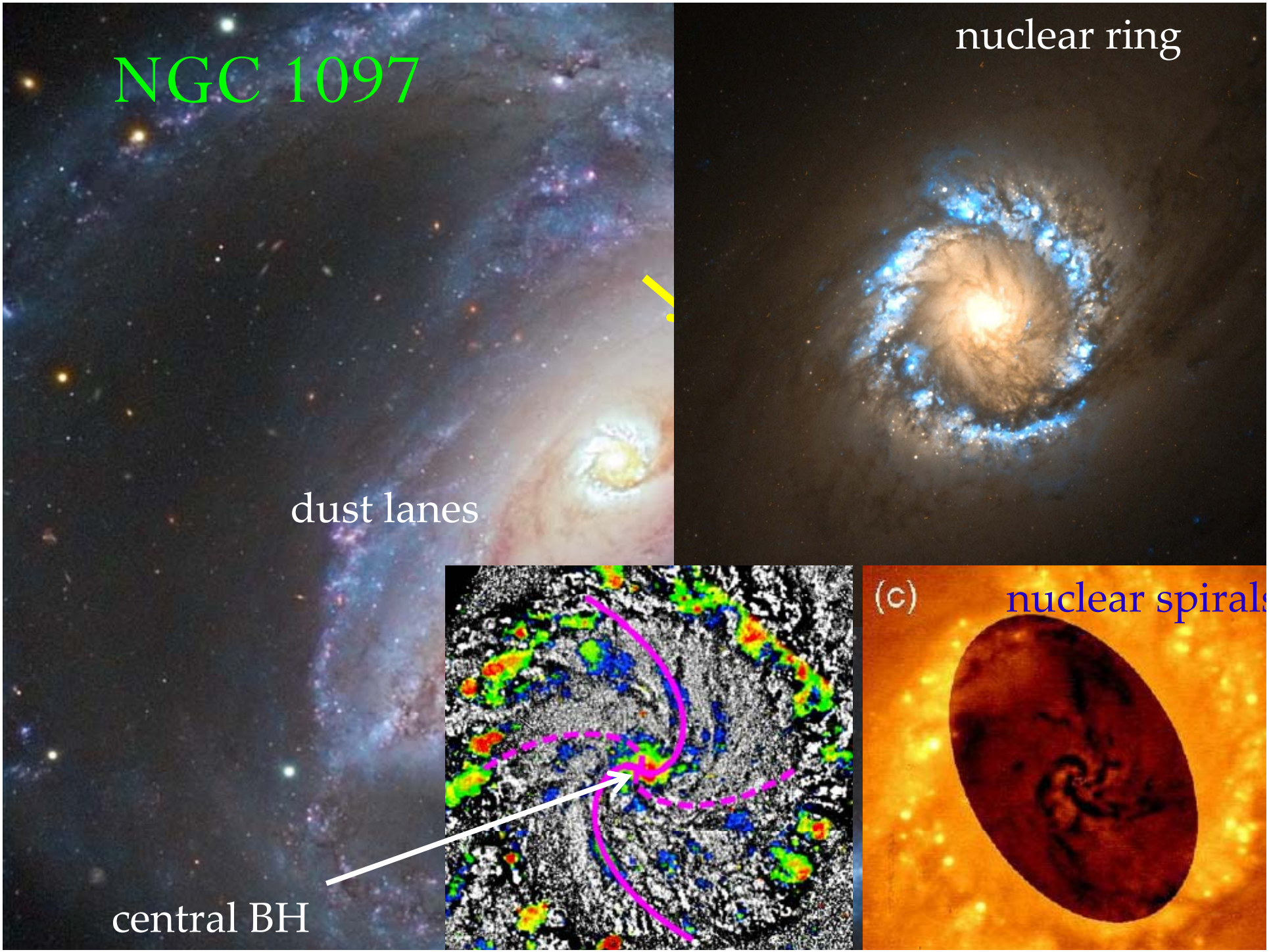
NGC 1097
nuclear ring
dust lanes
central BH
(c)
nuclear spirals

- Some galaxies have relatively straight dust lanes, while others have curved ones.

NGC 6951: $\Delta\alpha=9^{o}$

NGC 4321: $\Delta\alpha=73^{o}$

Comeron et al. (2009)

- Some galaxies have a relatively large nuclear ring, while others have smaller one.

NGC 1343: 1.2kpc × 0.9kpc

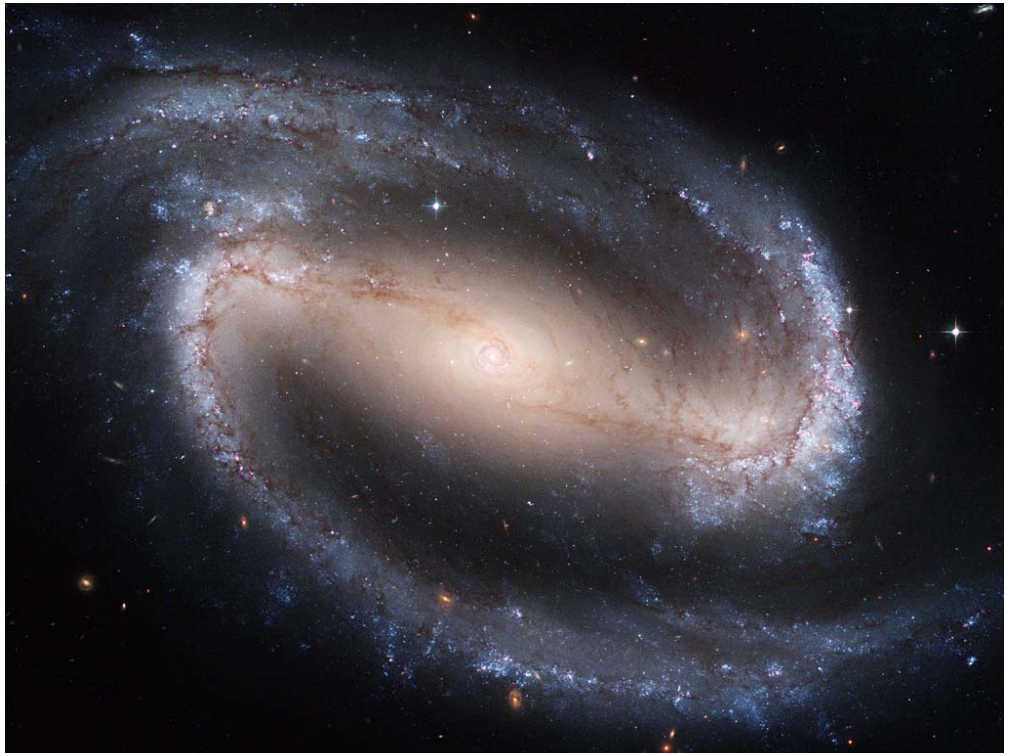

NGC 1300: 0.3kpc × 0.2kpc

Mazzuca et al. (2009)

- Some galaxies have tightly wound nuclear spirals, while others have loosely wound ones.

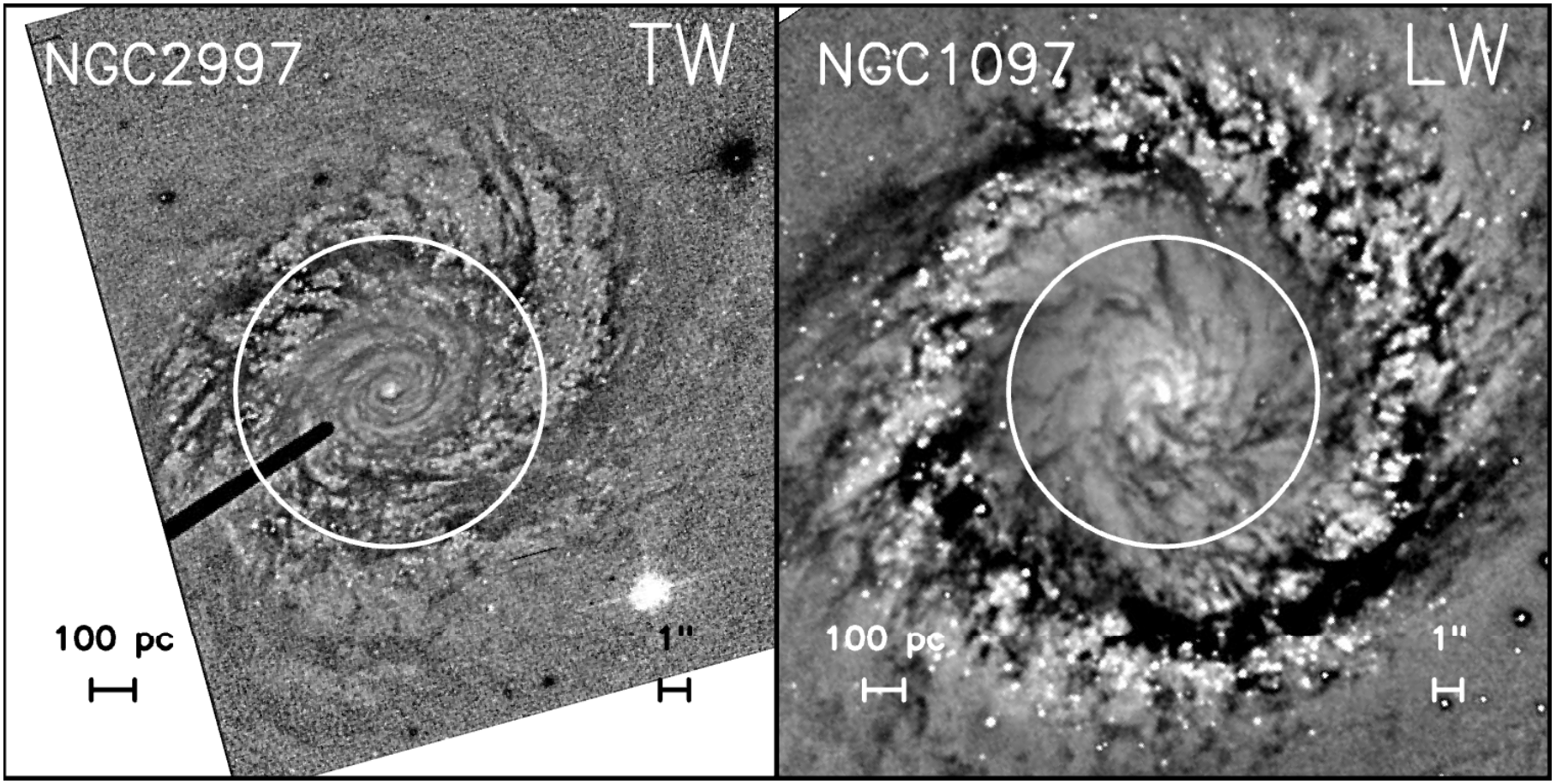

Peeples & Martini (2006)

Nuclear Rings

- Regarding nuclear rings, it has been widely accepted that rings form via **resonant interactions** of the gas with the bar potential.
  - This notion was driven by the fact that observed nuclear rings are located near the **inner Lindblad resonances** (e.g., Combes & Gerin 1985; Knapen et al. 1995; Comeron et al. 2010).
- Yet, there is no convincing theoretical argument.
  - Bar torque is very week near the ILRs.
  - Resonance is a secular process, occurring over a very long time scale.
  - Resonance tends to disperse the material, rather than gathering it (e.g., gaps in planetary rings and the asteroid belt).

Bar Model

- A normal galaxy with flat rotation at v_c~200 km/s in outer parts
  - M_{BH}= 4x10^7 $M_\odot$
- Bar : **a Ferrers ellipsoid**

$$\rho = \begin{cases} \rho_{\rm bar}\left(1-g^2\right)^n & \text{for } g<1, \\ 0 & \text{elsewhere,} \end{cases}$$
$$g^2 = y^2/a^2 + (x^2+z^2)/b^2$$

  - n=1 (cental density concentraion)
  - Semi-major axis ***a*=5 kpc**
  - Aspect ratio ***R*=*a*/*b* = 1.5 – 3.5**
  - Bar mass f_{bar} = $M_{bar}/(M_{bar}+M_{bulge})$ = **8%– 60%**
  - Ω_b = 33 km/s/kpc (R_{CO}=6kpc)

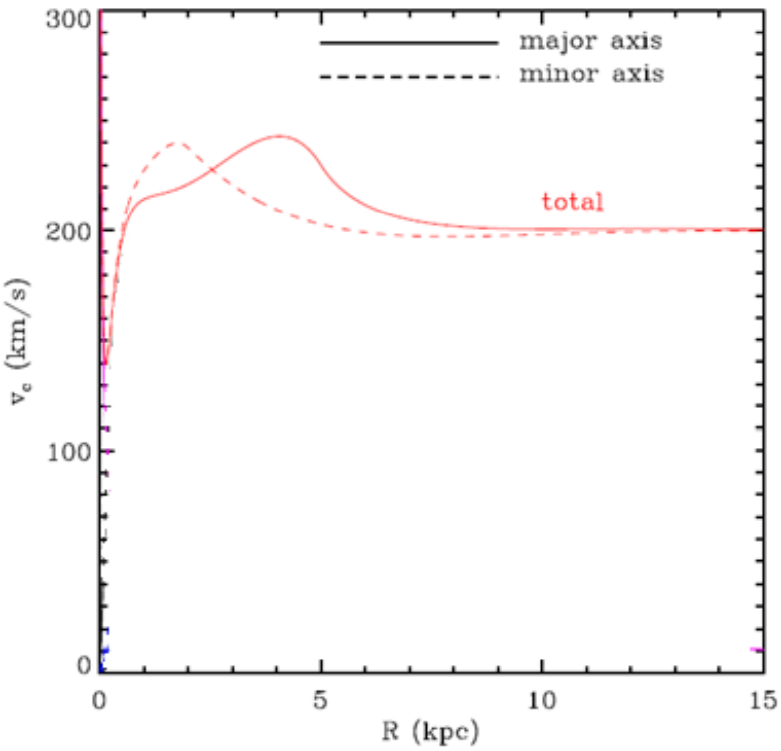

f_{bar}=30%
R=2.5,
M_{BH}=4x10^7 $M_\odot$

Bar Strength

- The most important parameter that controls the properties of bar substructures is the **bar strength Q_b** defined by

$$Q_b = \left. \frac{F_T}{F_R} \right|_{\max}$$

where F_T = tangential force due to a bar

F_R = radial force due to mass distribution

(e.g., Combes & Sanders 1981; Laurikainen & Salo 2002; Block et al. 2004; Laurikainen et al. 2004, 2006; Peeples & Martini 2006; Comeron et al. 2009, 2010)

- For our galaxy models with Ferrers bar,

$$Q_b = \begin{cases} 0.58\, f_{\rm bar}^{0.89}(a/b-1), & \text{for } n=0, \\ 0.44\, f_{\rm bar}^{0.87}(a/b-1), & \text{for } n=1, \\ 0.38\, f_{\rm bar}^{0.79}(a/b-1), & \text{for } n=2 \end{cases}$$

Bar Strength of Model Galaxies vs. Observations

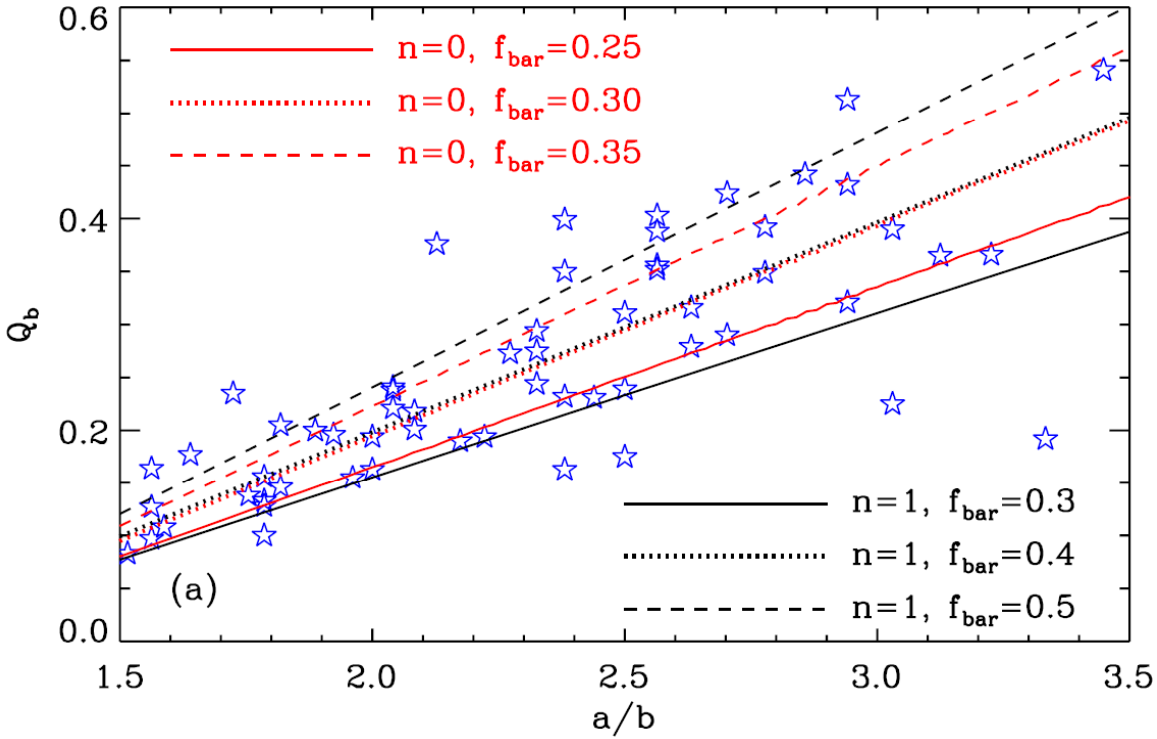

- The trend of Q_b becoming larger for a more elongagted bar in the observational estimates (Comeron et al. 2010) is consistent with the results of our galaxy models.
  - f_{bar} = 0.3–0.5 for n = 1
  - f_{bar} = 0.25–0.35 for n = 0

Numerical Method

- **CMHOG** Code (**C**onnection **M**achine **H**igher **O**rder **G**odunov)
  - Grid-based code in cylindrical geometry

- Logarithmically-spaced cylindrical grid with 1024x480 zones
- The bar is oriented along the *y*-axis.
- The gaseous disk is self-gravitating and isothermal (c_s=10 km/s) without magnetic fields.
- The ideal HD equations are solved in a frame rotating with the bar.
- No back reaction of the gas to the stellar bar.
- In order to avoid strong trasients, the amplitude of the bar potential is slowly incrased over ~200 Myr.

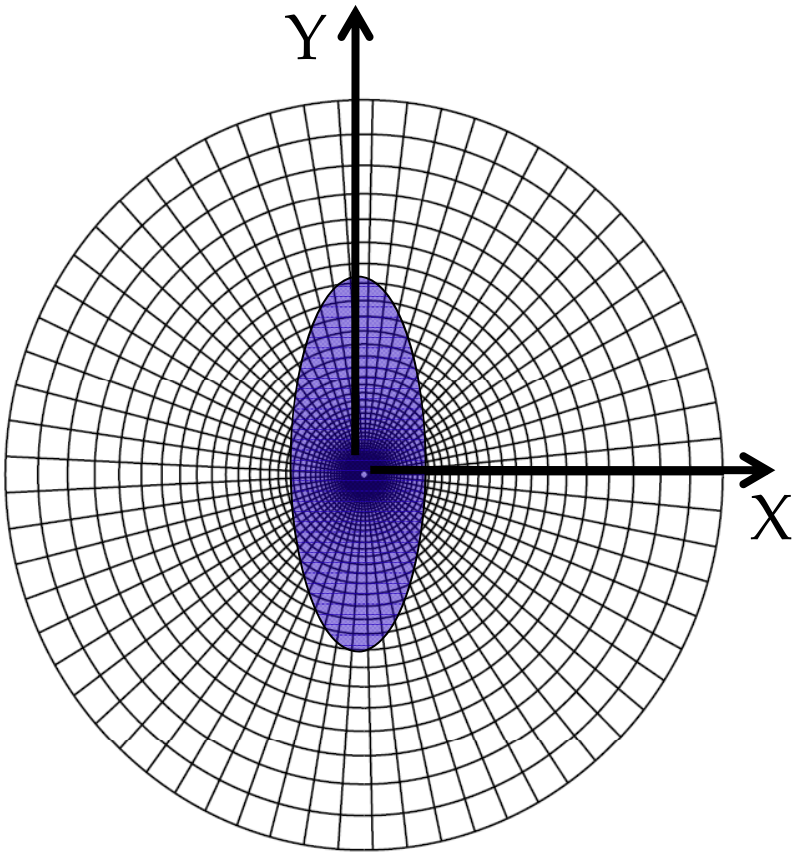

x_1 and x_2 Orbits

- In the presence of an non-axisymmetric potential, angular momentum is not conserved, while **Jacobian integral** defined by

$$E_J = \frac{1}{2}|\dot{r}|^2 + \Phi_{\text{eff}}$$

  is conserved.

- Two (prograde) closed-orbit families in the rotating frame (Contopoulos & Papayannopoulos 1980):
  - **x_1 orbits** elongated along the bar major axis
    - Support the bar potential.
    - Associated with dust lanes.
  - **x_2 orbits** aligned along the bar minor axis
    - Associated with nuclear rings.

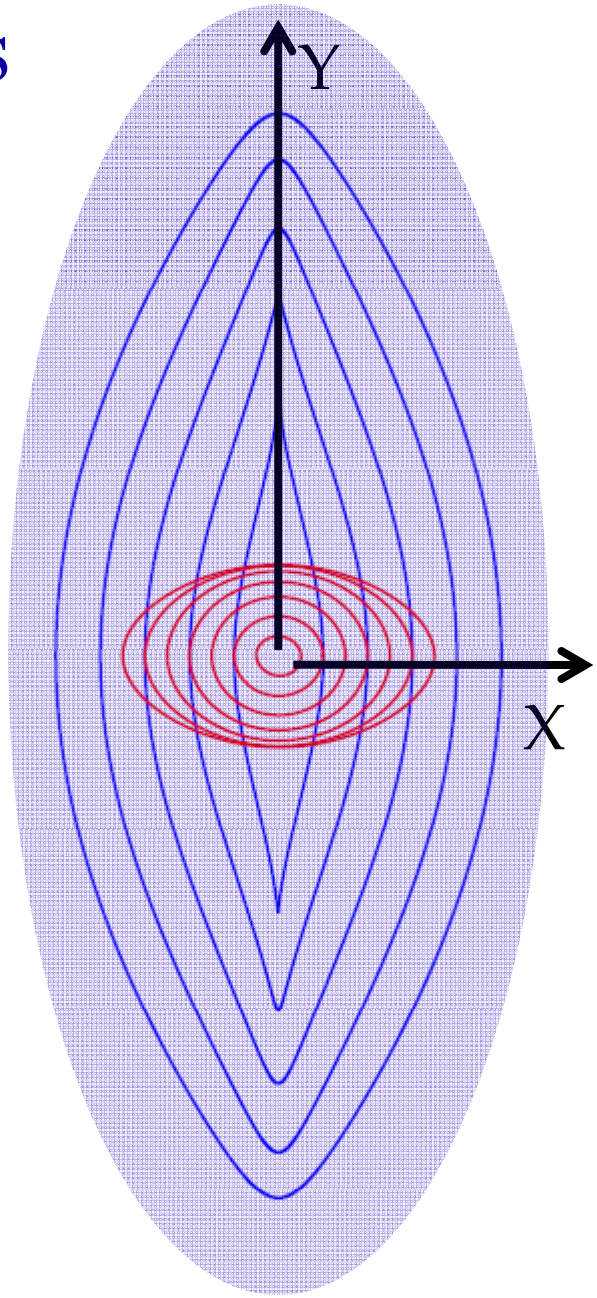

Model with Q_b=0.23

Kim et al. (2012)

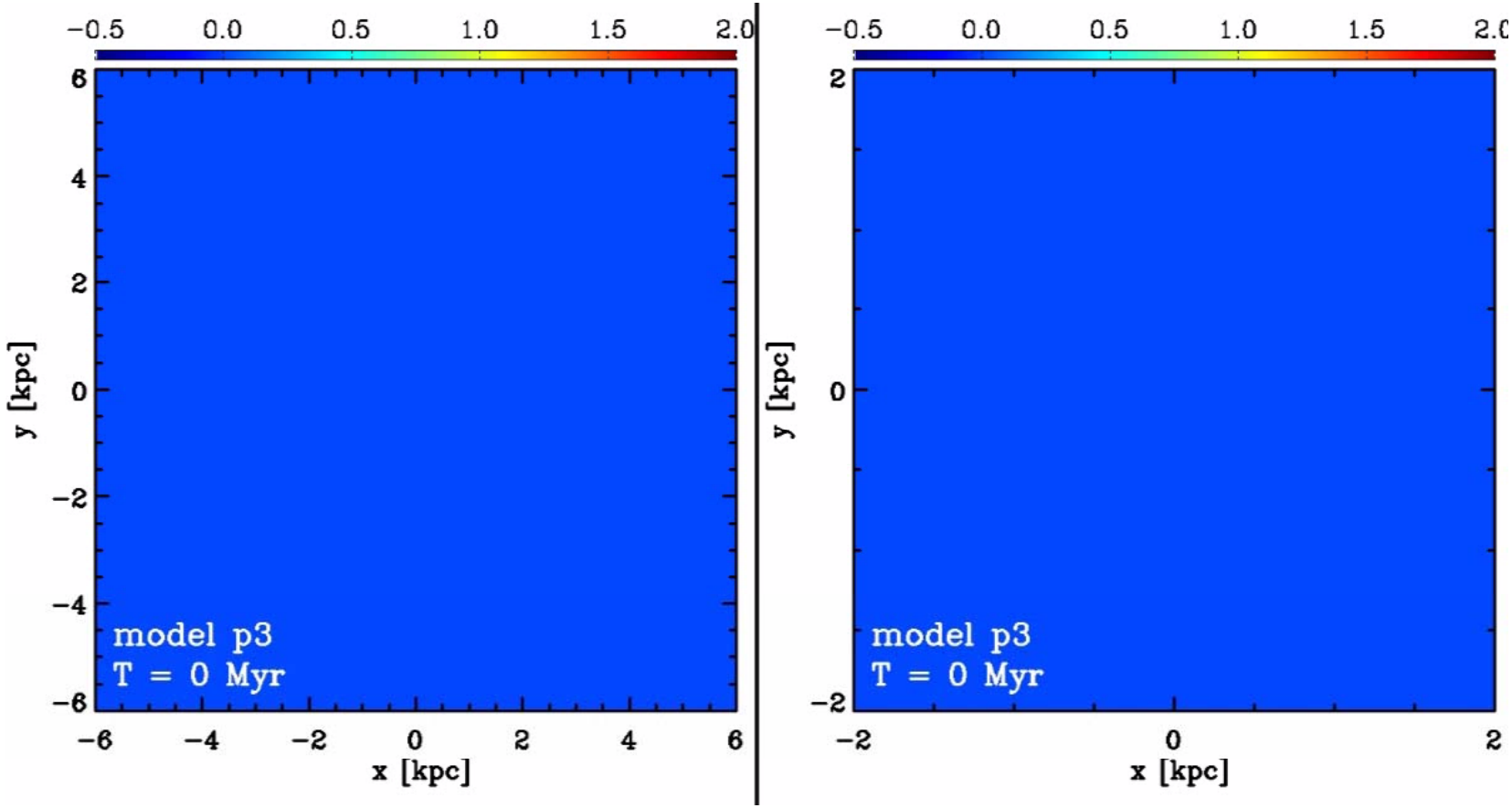

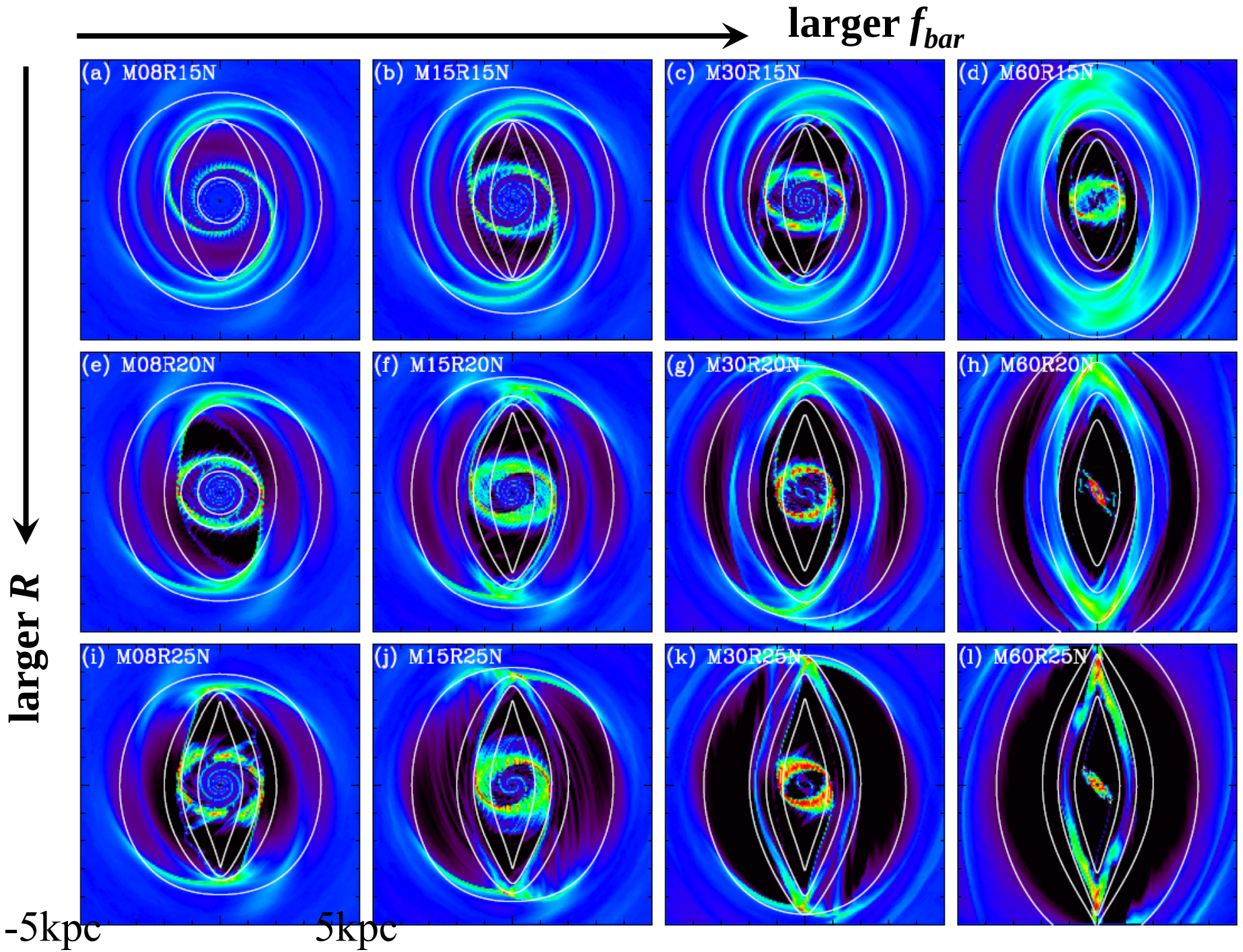
larger f_{bar}
larger R
(a) M08R15N
(b) M15R15N
(c) M30R15N
(d) M60R15N
(e) M08R20N
(f) M15R20N
(g) M30R20N
(h) M60R20N
(i) M08R25N
(j) M15R25N
(k) M30R25N
(l) M60R25N
-5kpc
5kpc

Curvature $\Delta\alpha$ of Dust Lanes

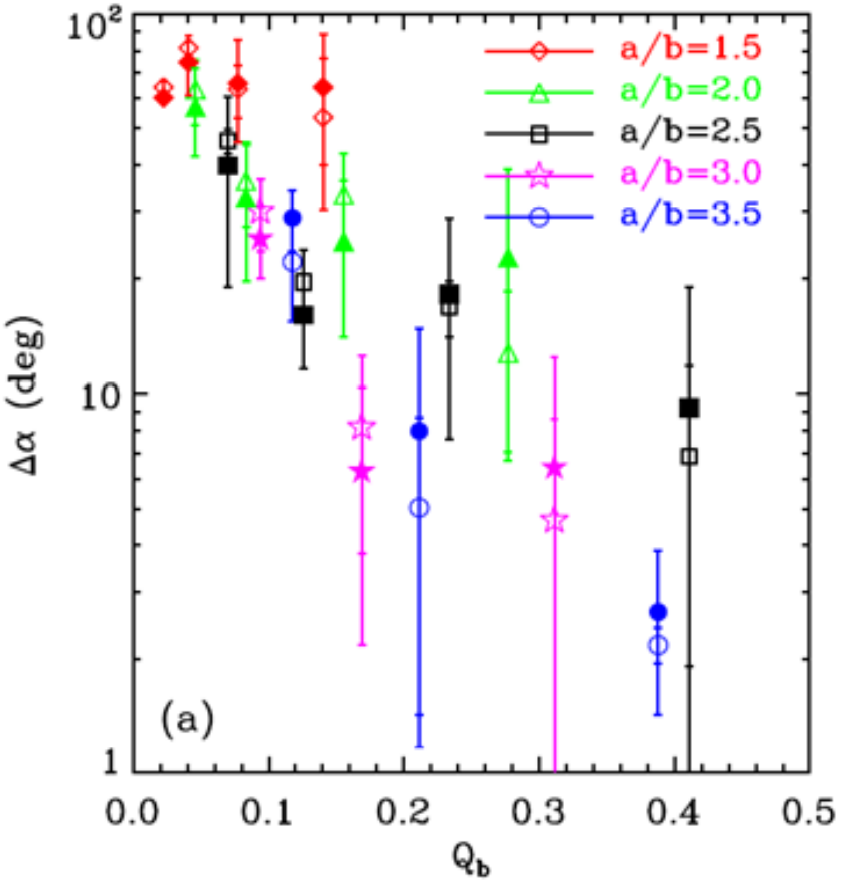

(Average is taken over 250-350 Myr)

- Overall, the shape of dust lanes is well described by x_1 orbits.
- A stronger and more elongated bar has more straight dust lanes (Athanassoula 1992; Knapen et al. 2002; Comeron et al. 2009).

Strength of Dust Lanes

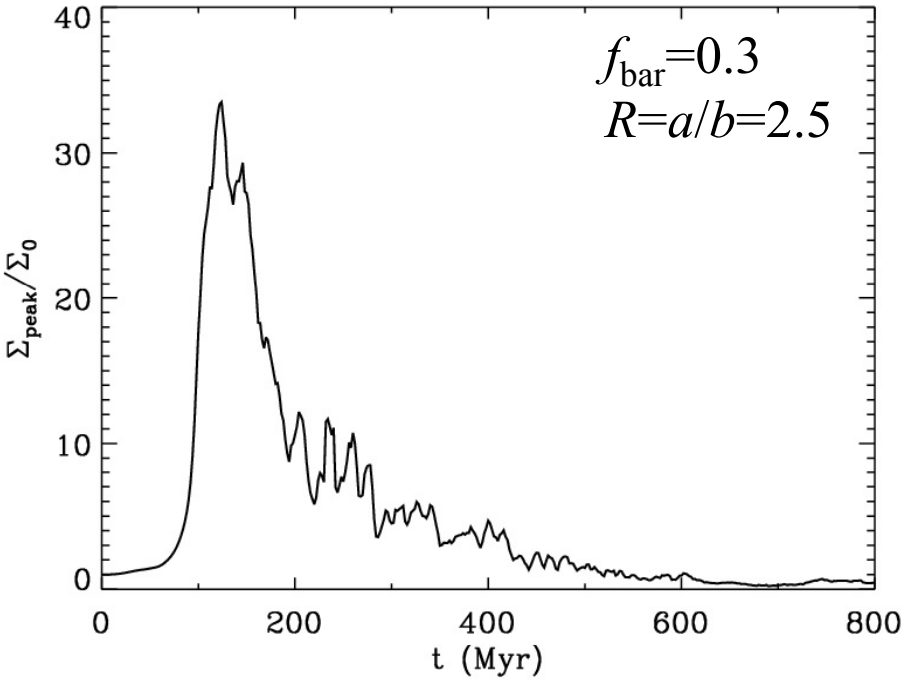

- Dust lanes remain strong only for 100 Myr before the bar potential achieves the full strength.
  - The rapid decline of the strength of dust lanes is primarily due to the fact that the gas only inside the outermost x_1-orbit can respond strongly to the bar potential to lower its orbits.

Ring Formation

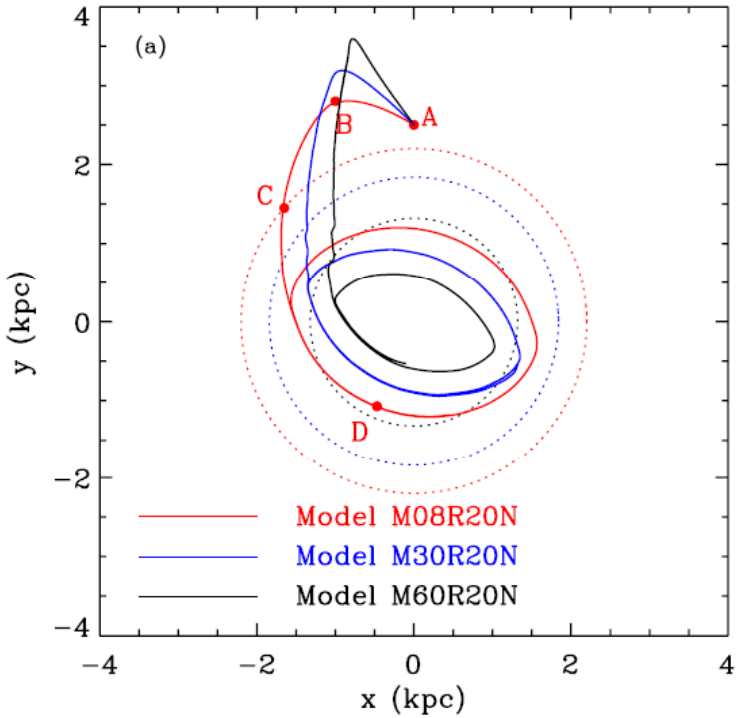

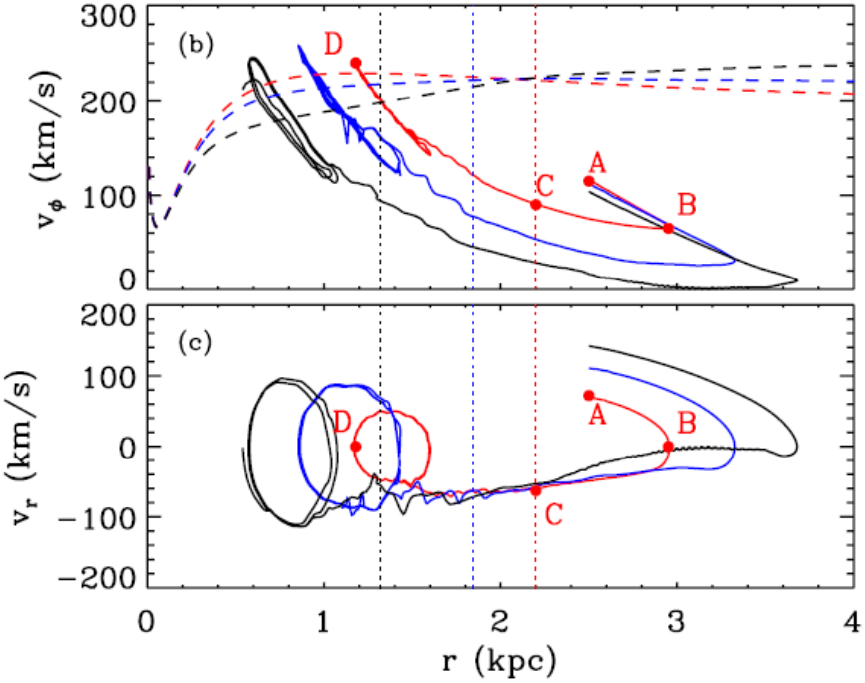

- The inflowing speed is so large that the bar torque cannot stop gas motions across the ILR.
- The inflowing gas keeps moving in and eventually forms a nuclear ring at the location where the centrifugal force balances the external gravitational force.

Nuclear Rings

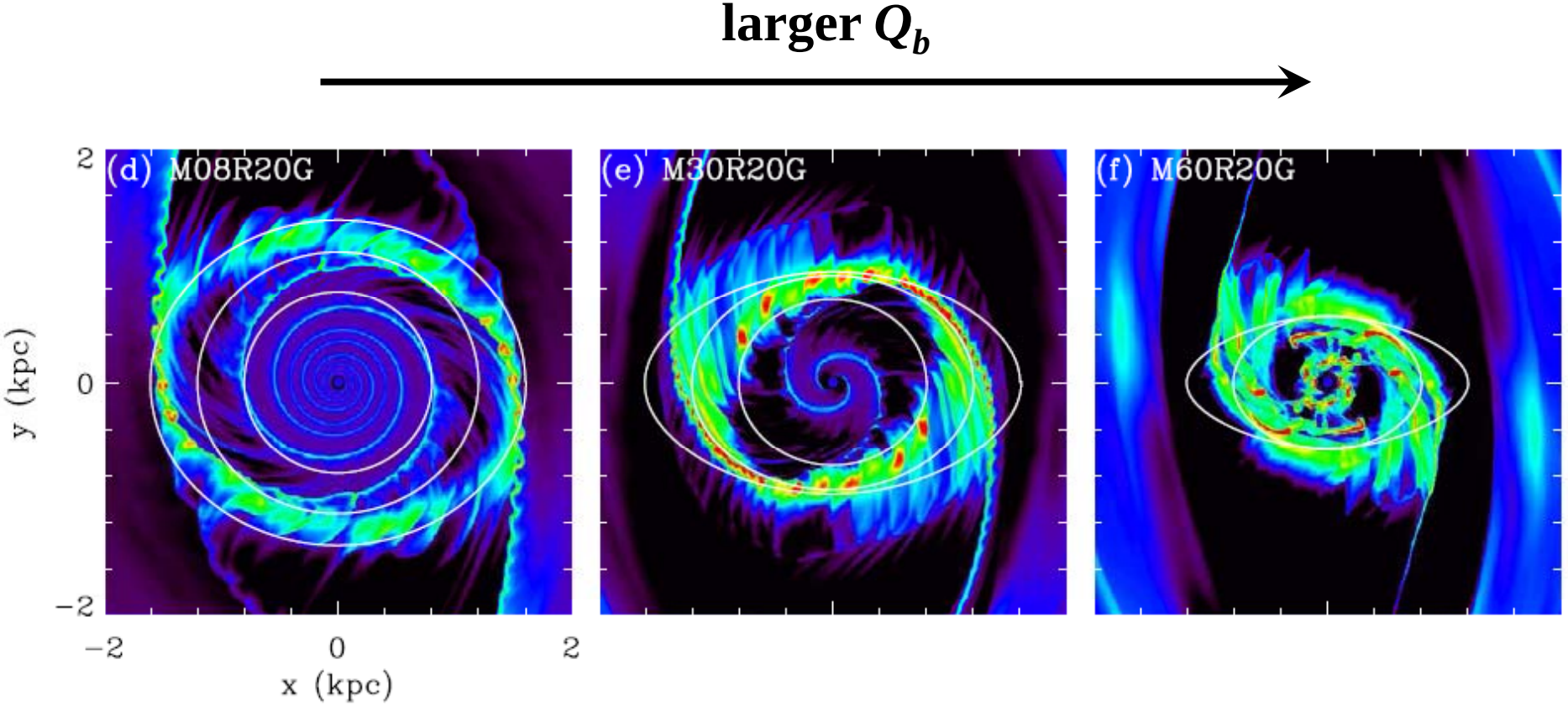

Ring Size

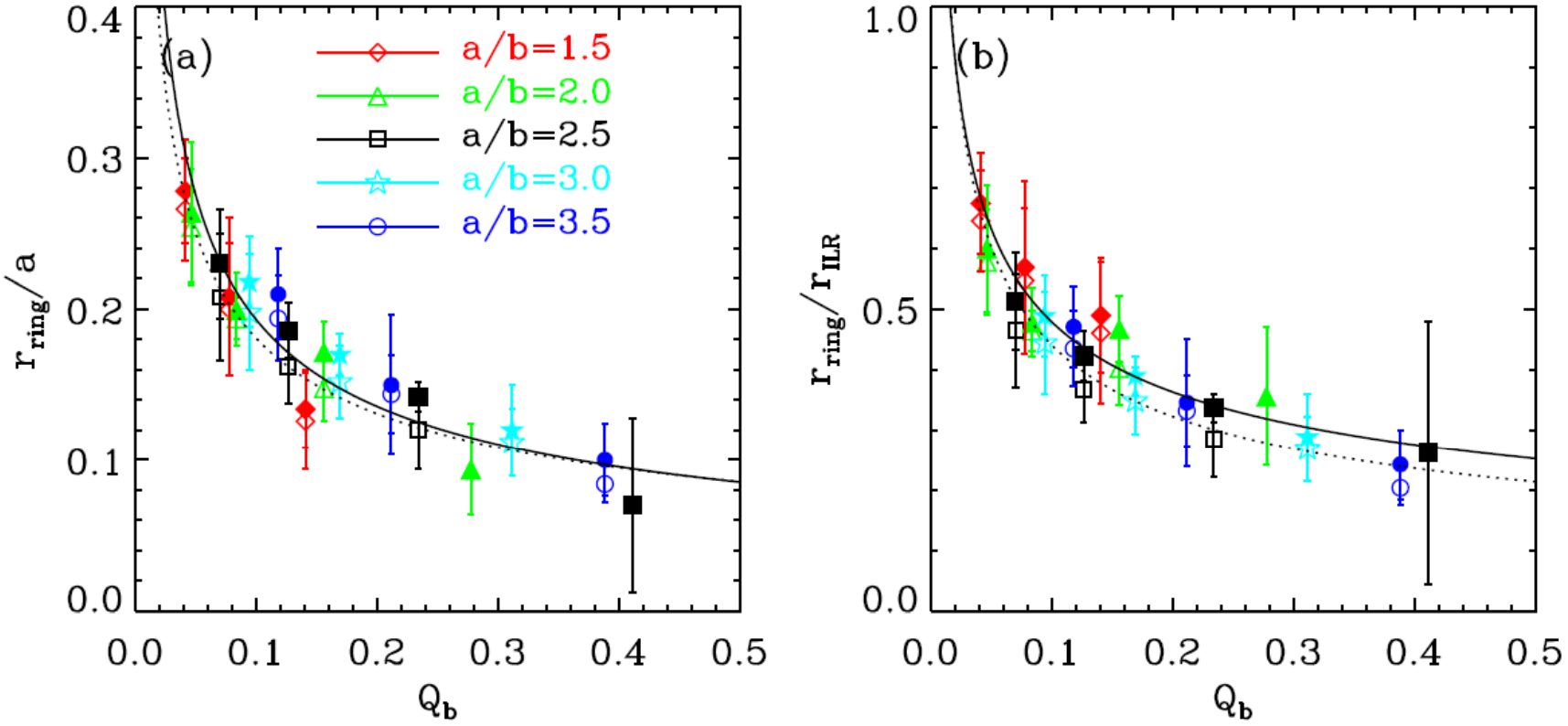

- The ring position is in general inside the inner Lindblad resonance of the bar potential.
- Rings are smaller in models with a stronger bar.

Comparison With Observed Ring Sizes

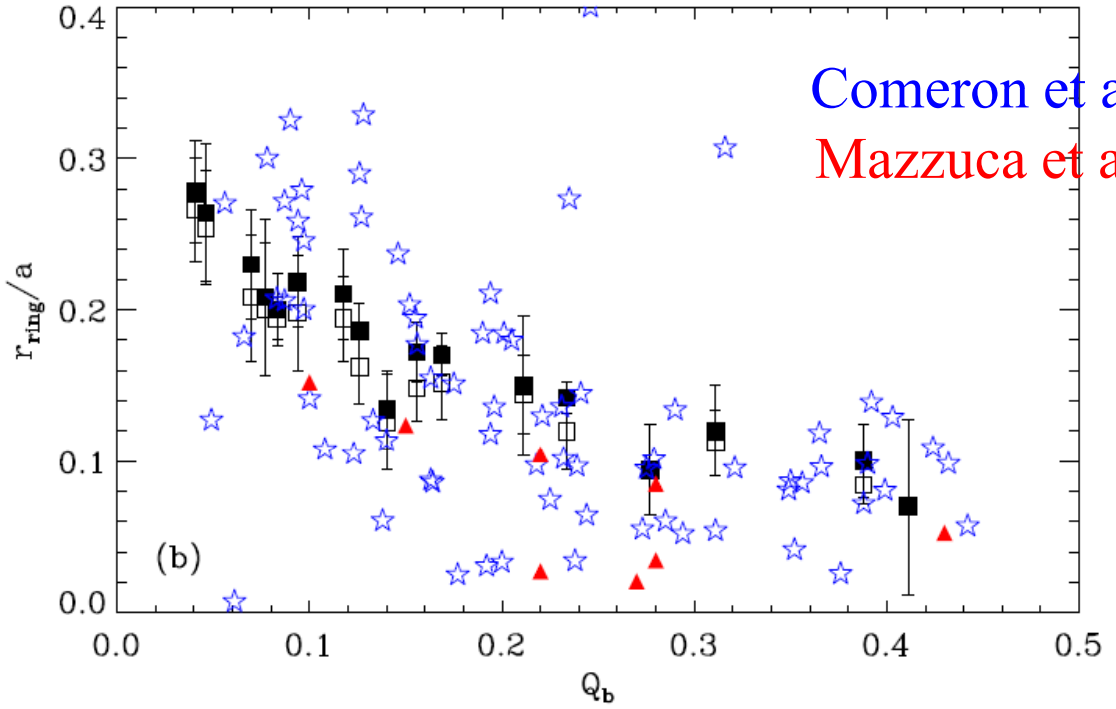

- Both observational and numerical results show that stronger bars can possess smaller rings.
- For $Q_b < 0.15$, the agreement between observational and numerical results is quite good.
- For $Q_b > 0.15$, the ring size in our models corresponds roughly to the upper envelope of the observational results.

Star Formation In Nuclear Rings

Model with Σ=20 $M_{\odot}$ pc^{-2} (Seo & Kim 2013)

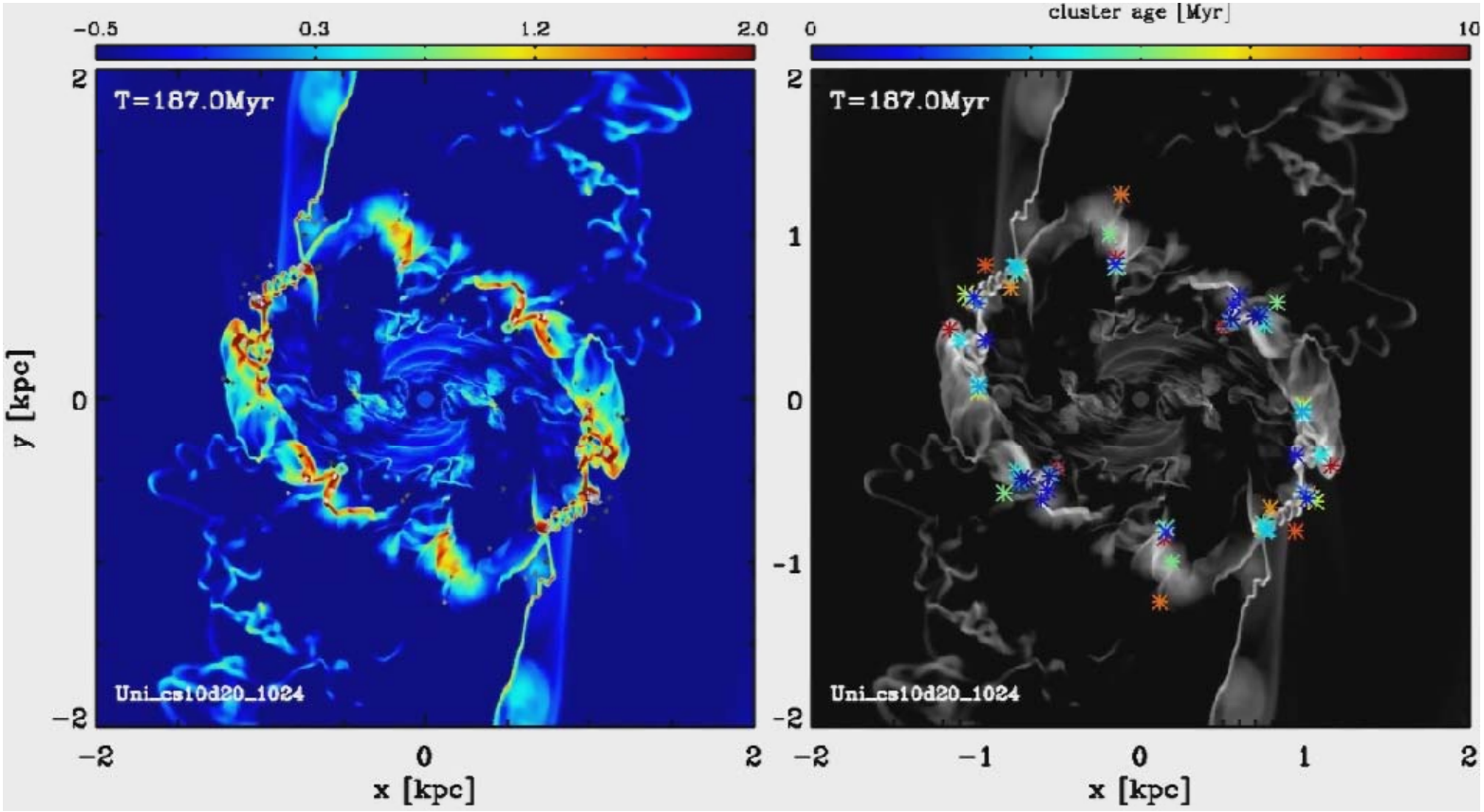

Ring Star Formation Rate

- Star formation rate in the nuclear rings is well correlated with the mass inflow rate to the rings.
- SFR shows a strong primary burst lasting for about 100 Myr and then decays to small values below $\sim 1 M_{\odot}\ yr^{-1}$.
  - Contrast to observational results that show that ring star formation is long lived lasting for 1-1.5 Gyr, with multiple episodes (Allard et al. 2006; Sarzi et al. 2007; van der Laan et al 2013)

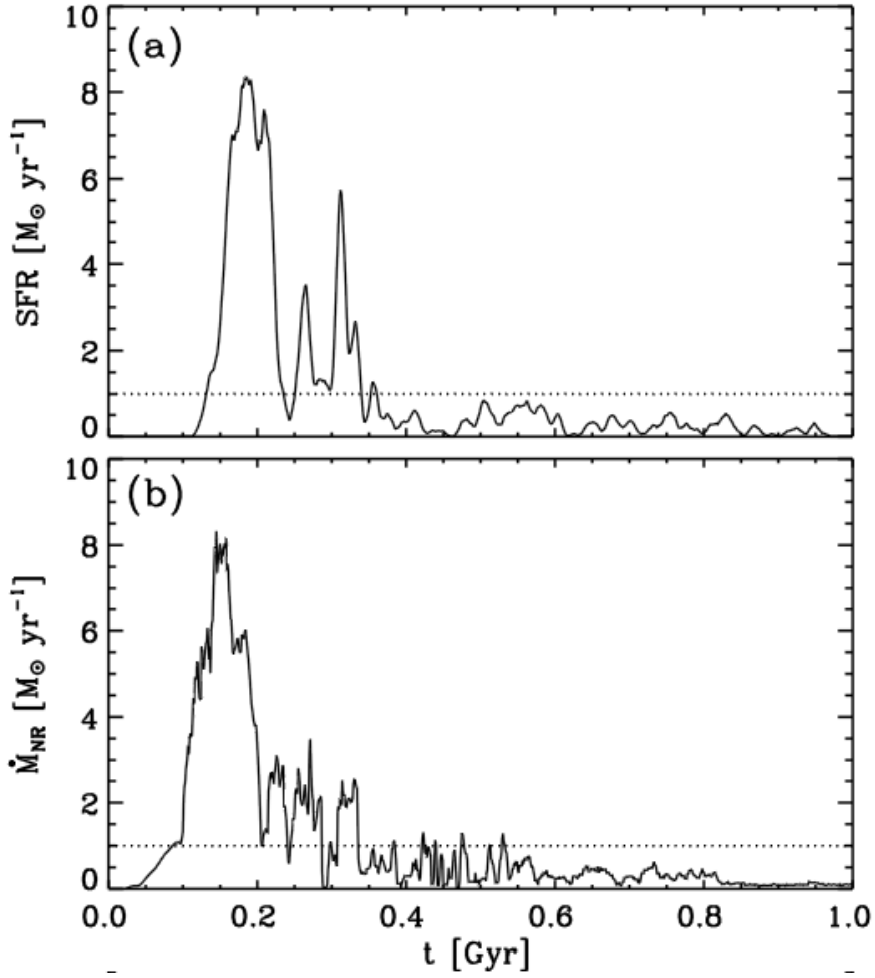

Necessity of Gas Feeding to the Bar Region

- The gas in the bar regions should be replenished continuously or continually in order to explain observed **strong dust lanes** as well as **prolonged SF** in nuclear rings of barred galaxies.
- Candidate mechanisms for gas feeding
  - angular momentum dissipation by spiral arms (Roberts & Shu 1972; Lubow et al. 1986; Hopkins & Quataert 2011)
  - galactic fountains (e.g., Fraternali & Binney 2006, 2008).
  - cosmic accretion of primordial gas (e.g., Dekel et al. 2009)
    - HVCs, ~ 0.7 $M_\odot$ yr^{-1} for M31/Milky-Way-type galaxies (Richter 2012)
- We study the first possibility directly including a spiral potential in our numerical models.

Models With a Bar and Spiral Arms

- Most barred galaxies have spiral arms at outer regions, as well.
- Some galaxies appear to have a bar and spiral arms rotating at a similar pattern speed, while they have different pattern speeds in other galaxies (Sellwood & Sparke 1988; Fathi et al. 2009; Martinez-Garcia et al. 2011)

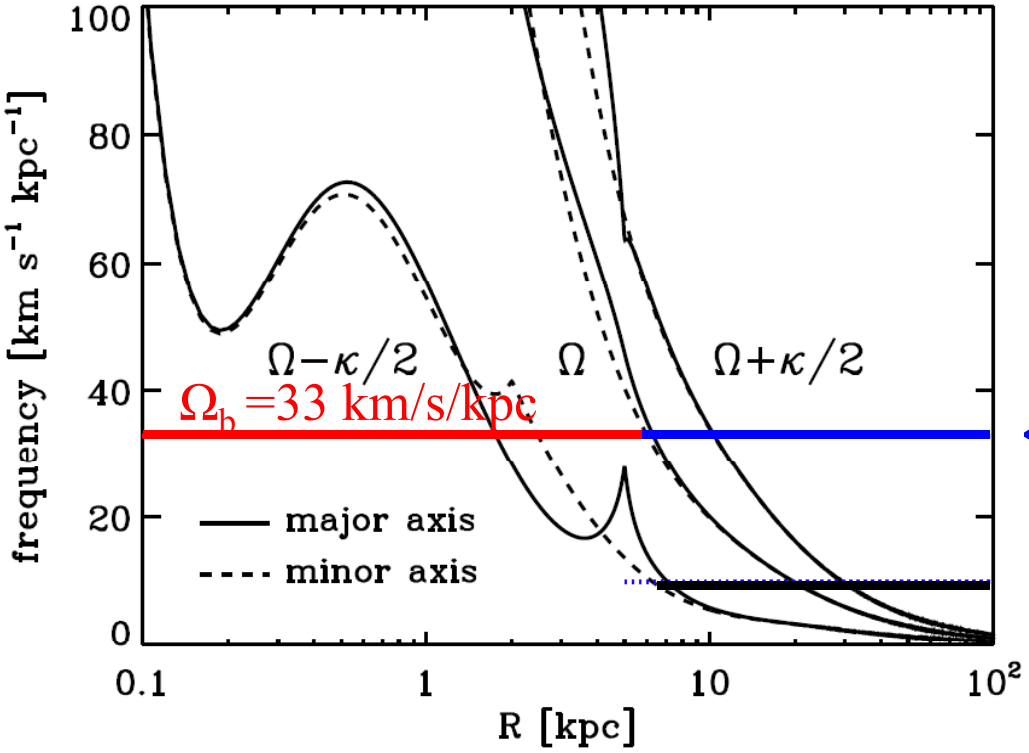

$\Omega_s=\Omega_b$ (EQ Models)

$\Omega_s\neq\Omega_b$ (DF Models)

Spiral Arm Potential

- Logarithmic spirals (Local analog of Lin & Shu 1964, 1966)

$$\Phi_s(R,\phi;t) = \Phi_{s0}\cos\left(m\left[\phi + \frac{\ln R}{\tan p_*} - \Omega_s t + \phi_0\right]\right)$$

  over R=5 kpc to 30 kpc
  - p_* (=20°): pitch angle of the stellar pattern
  - m (=2): number of arms
- Arm strength is controlled by the dimensionless parameter

$$\mathcal{F} \equiv \frac{m\Phi_{s0}}{v_c^2 \tan p_*} = 5\text{-}20\%$$

  (Roberts 1969; Shu, Milione, & Roberts 1973)
- Pattern speed of the spiral arms
  - Ω_s = 33 km/s/kpc (EQ Models) : CR at R=6 kpc
  - Ω_s = 10 km/s/kpc (DF Models) : CR at R=19.8 kpc
- All simulations are run in a framing corotating with the bar.

EQ Model with $\mathcal{F}$=10%

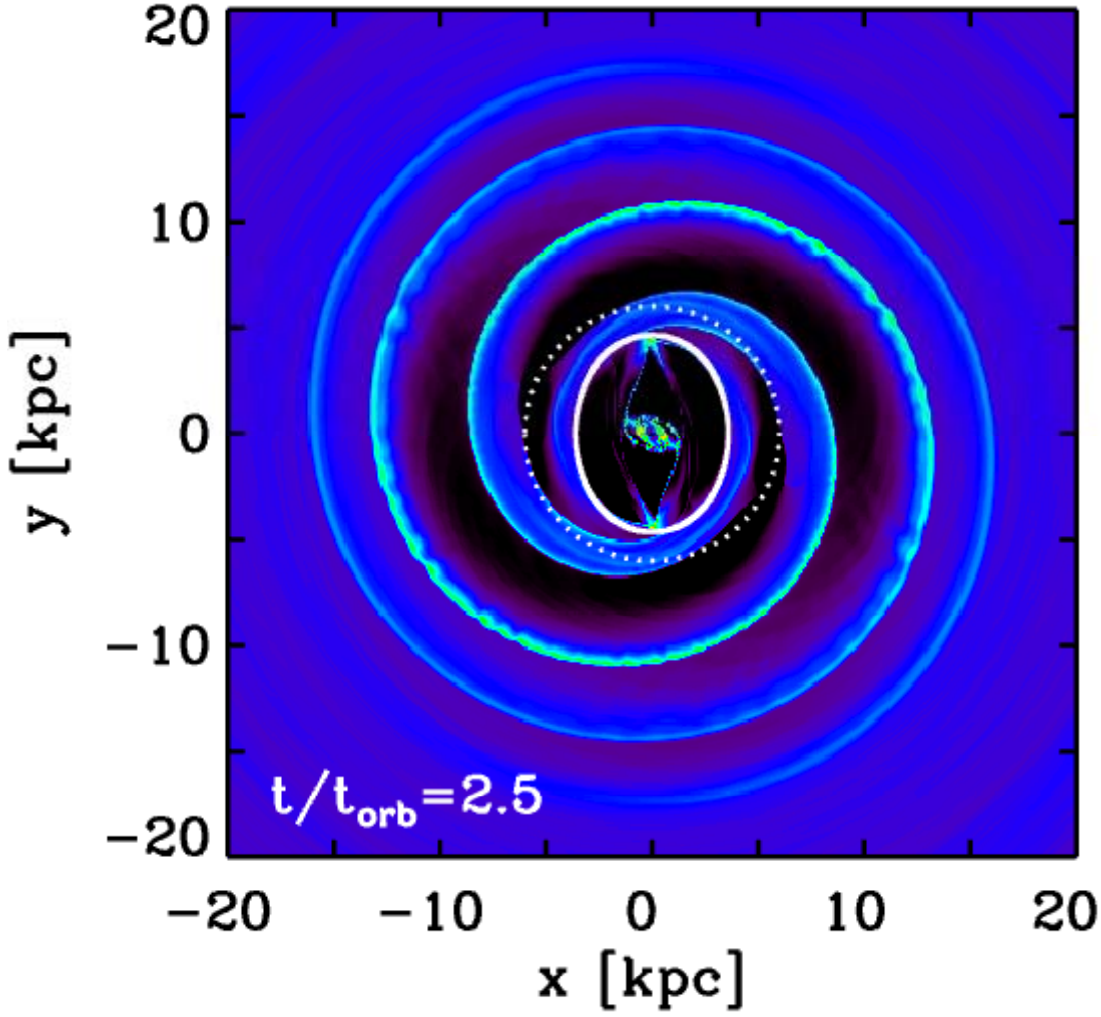

Kim & Kim (ApJ, submitted)

DF Model with $\mathcal{F}$=10%

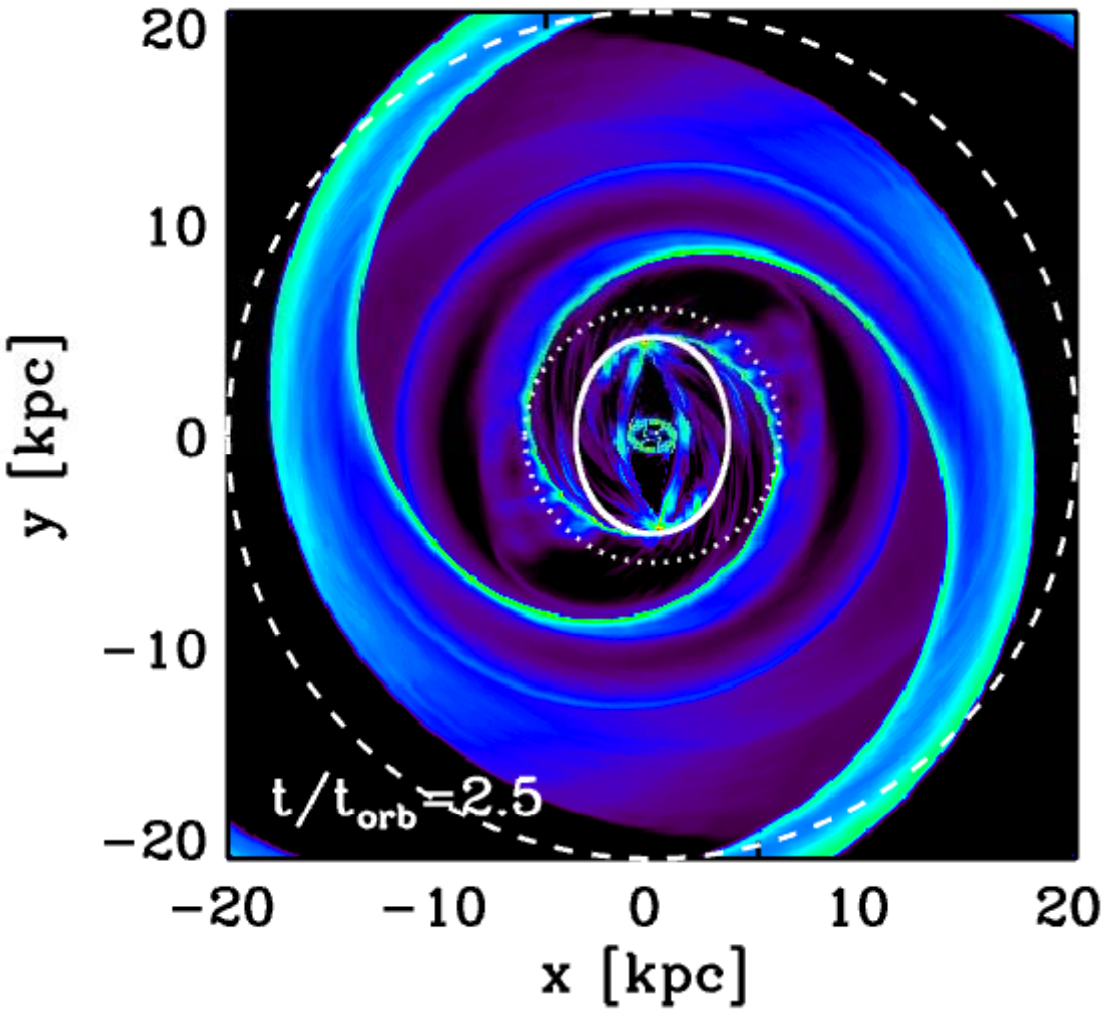

Kim & Kim (ApJ, submitted)

Resonant Features

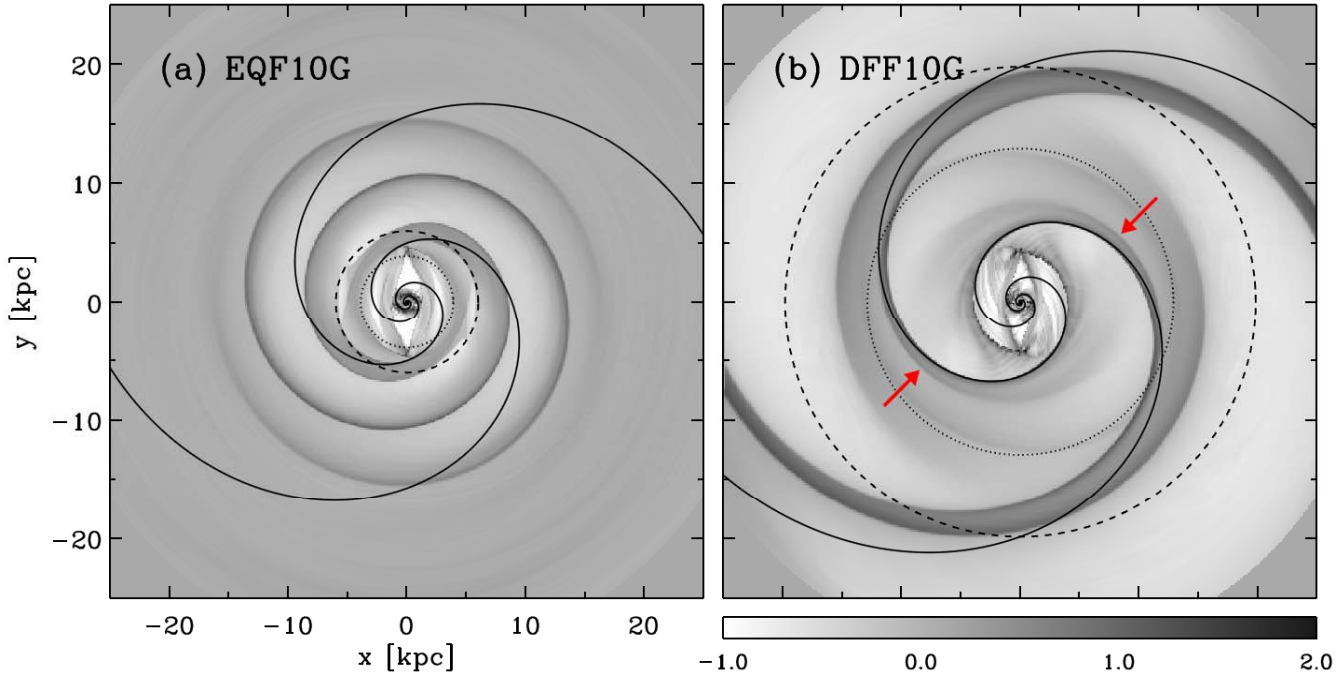

- In the DF models, weak features develop from the arms near the 4/1 resonance, similarly to *spurs* identified by Chakrabarti et al. (2003).
  - In the EQ models, any features that may grow are overwhelmed by the bar potential.
- No other resonance features such as branchings, bifurcations, etc., which seem to require spiral arms to be relatively loosely wound with $p_* > 30^o$ (e.g., Patsis et al. 1994, 1997; Chakrabarti et al. 2003; Yanez et al. 2008).

Extent and Shape of Gaseous Arms

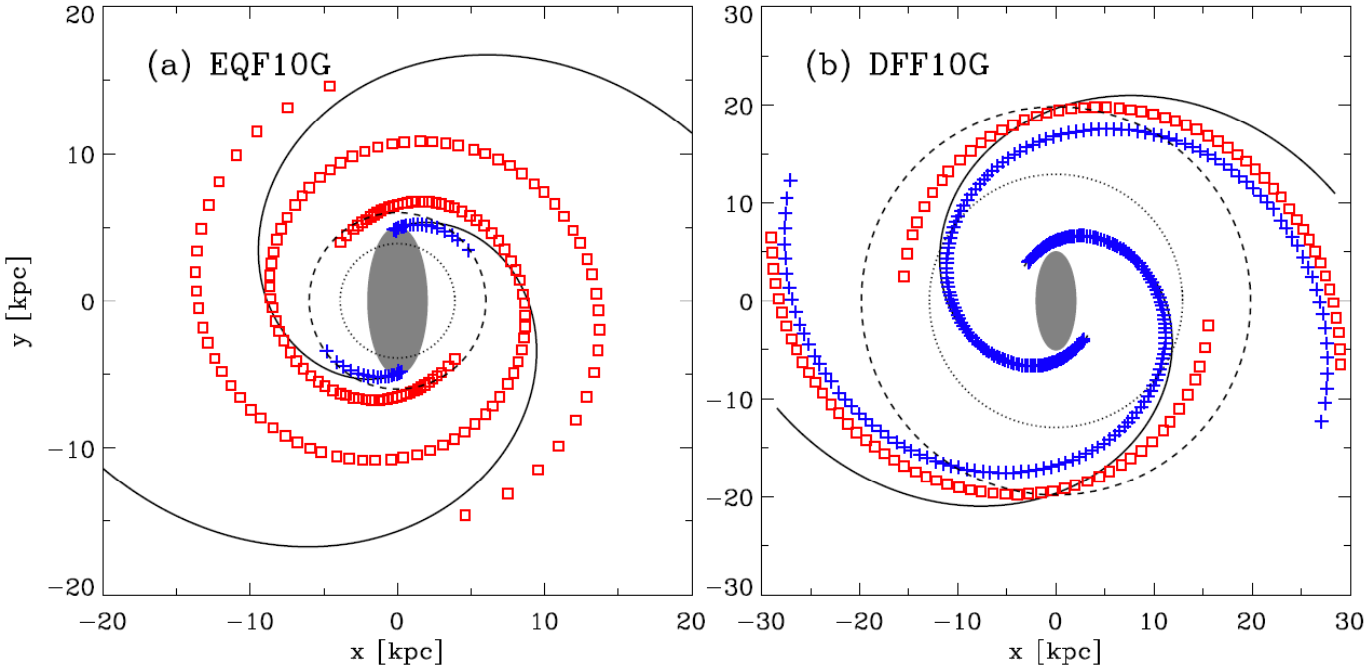

□: shocks by the gas outside the CR

＋: shocks by the gas inside the CR

- Extension of spiral shocks
  - EQ models: only up to R=15 kpc
  - DF models: all the way to the outer radial boundary
- Pitch angle of gaseous arms, $p_{\rm gas}$
  - $p_{\rm gas} << p_*$ in the EQ models
  - $p_{\rm gas} \leq p_*$ in the DF models

Perpendicular Mach Number of Spiral Shocks

- The time interval between two successive passages of the spiral arms: $t_{\rm arm} = \pi/|\Omega - \Omega_{\rm s}|$,
- The arm-to-arm sound crossing time : $t_{\rm sound} = \pi R/c_s$.
- If $t_{\rm sound}/t_{\rm arm} = \mathcal{M}_\perp / \sin p_* > 30$, the gas does not have sufficient time to adjust itself to one arm before encountering the next arm.
  - the rapid rotation of the potential effectively makes itself smoothed significantly along the azimuthal direction.

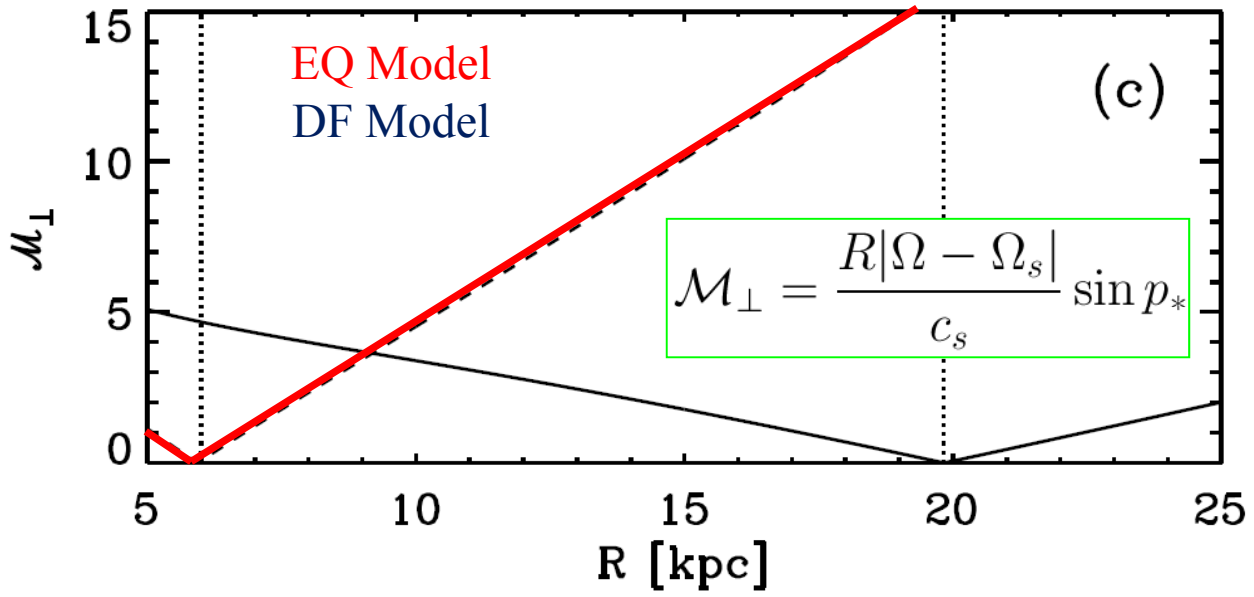

Pitch Angles of Gaseous Arms

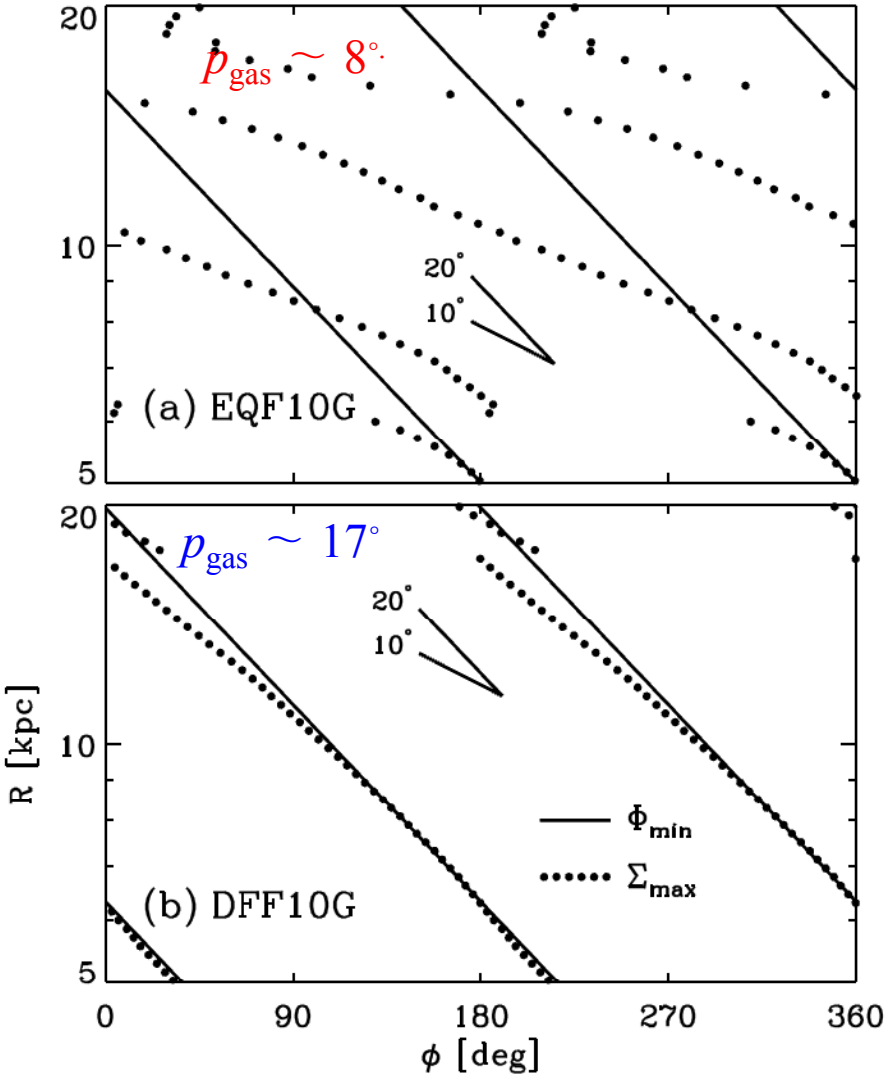

- In a quasi-steady state, stronger spiral shocks tend to form at farther downstream. (Kim &Ostriker 2002; Gittins & Clark 2004)
- In EQ models, $\mathcal{M}$ ... vary

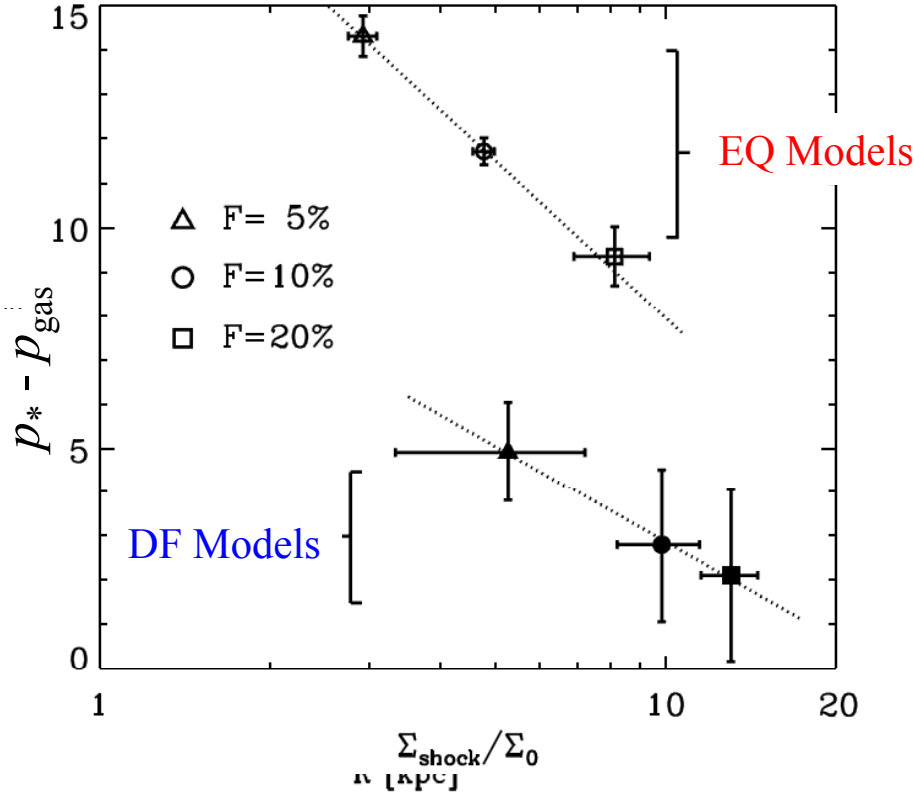

Observed Arm Pitch Angles

Grosbol & Patsis (1998)

Galaxy	Pitch angle i_2 K′	I	V	B	Δ	range
NGC 3223	-8°.8	-9°.4	-8°.8	-8°.7	0°.5	25-36″
NGC 5085	-17°.4	-13°.0	-11°.7	-10°.9	0°.5	25-40″
NGC 5247	-34°.1	-31°.8	-29°.9	-27°.4	0°.7	30-50″
NGC 5861	-12°.4	-11°.8	-11°.9	-	0°.5	20-35″
NGC 7083	-22°.1	-20°.3	-17°.6	-15°.0	1°.0	11-18″

Martinez-Garcia (2012)

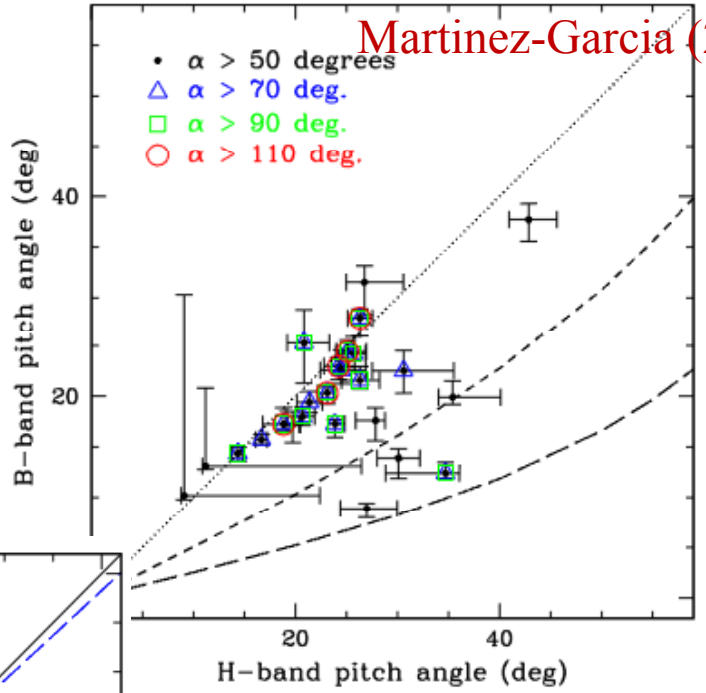

Seigar et al. (2006)

$$P_{\rm NIR} = (0.50 \pm 1.25) + (0.98 \pm 0.04) P_{\rm opt}$$

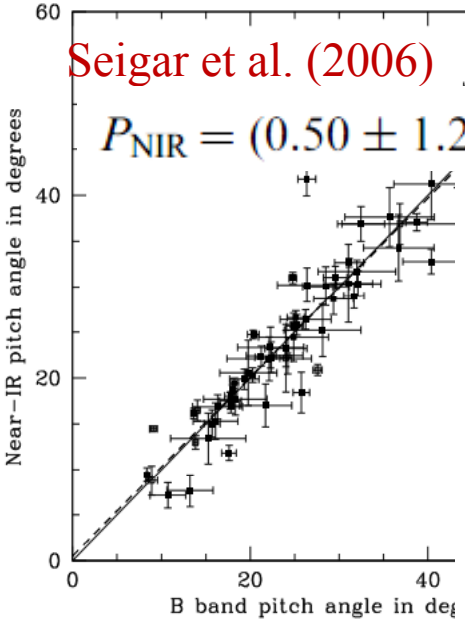

Davis et al. (2012)

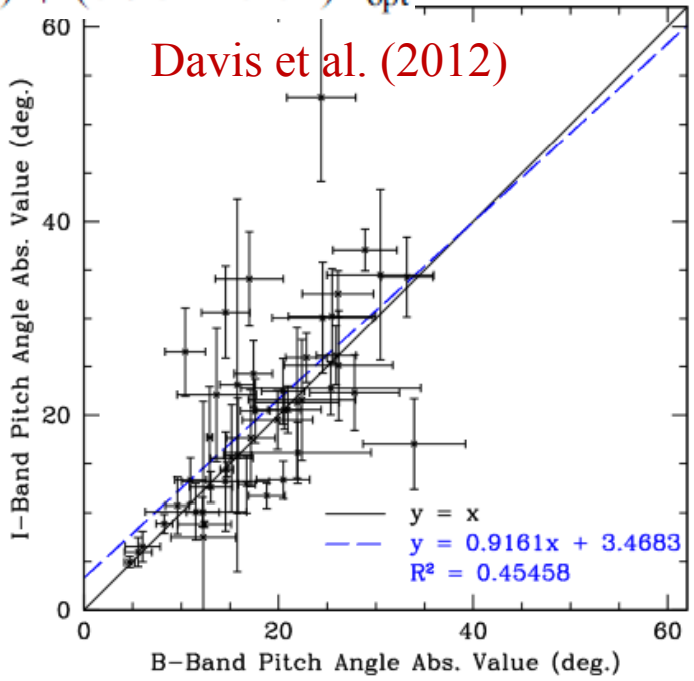

- Overall, $p_{\rm gas}$ is smaller by ~2° than p_* for p_* ~ 10° - 30°, despite almost 1:1 relations between them.

Radial Mass Drift

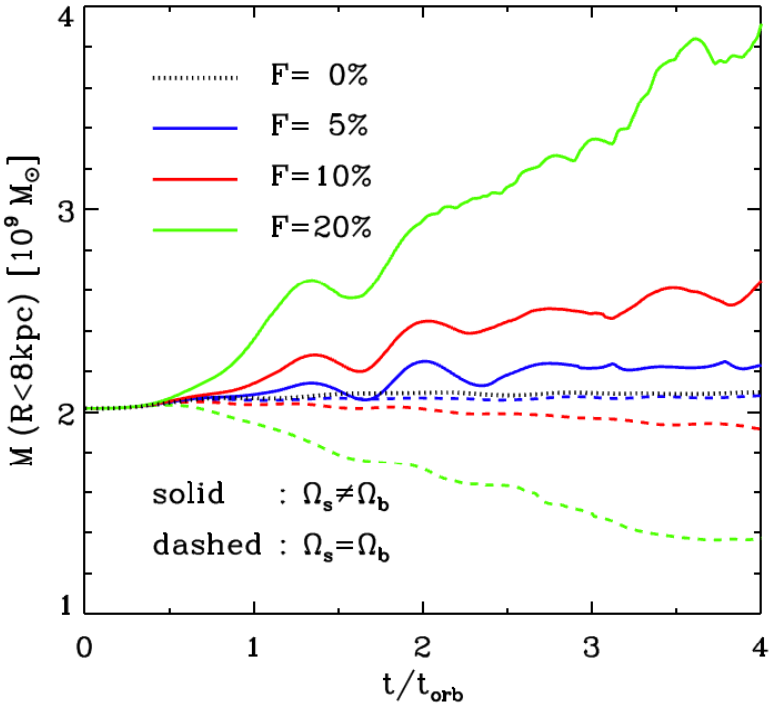

- Temporal changes of the gas mass within 8 kpc

$$M_{\rm tot} = \frac{dM(R)}{dt}$$

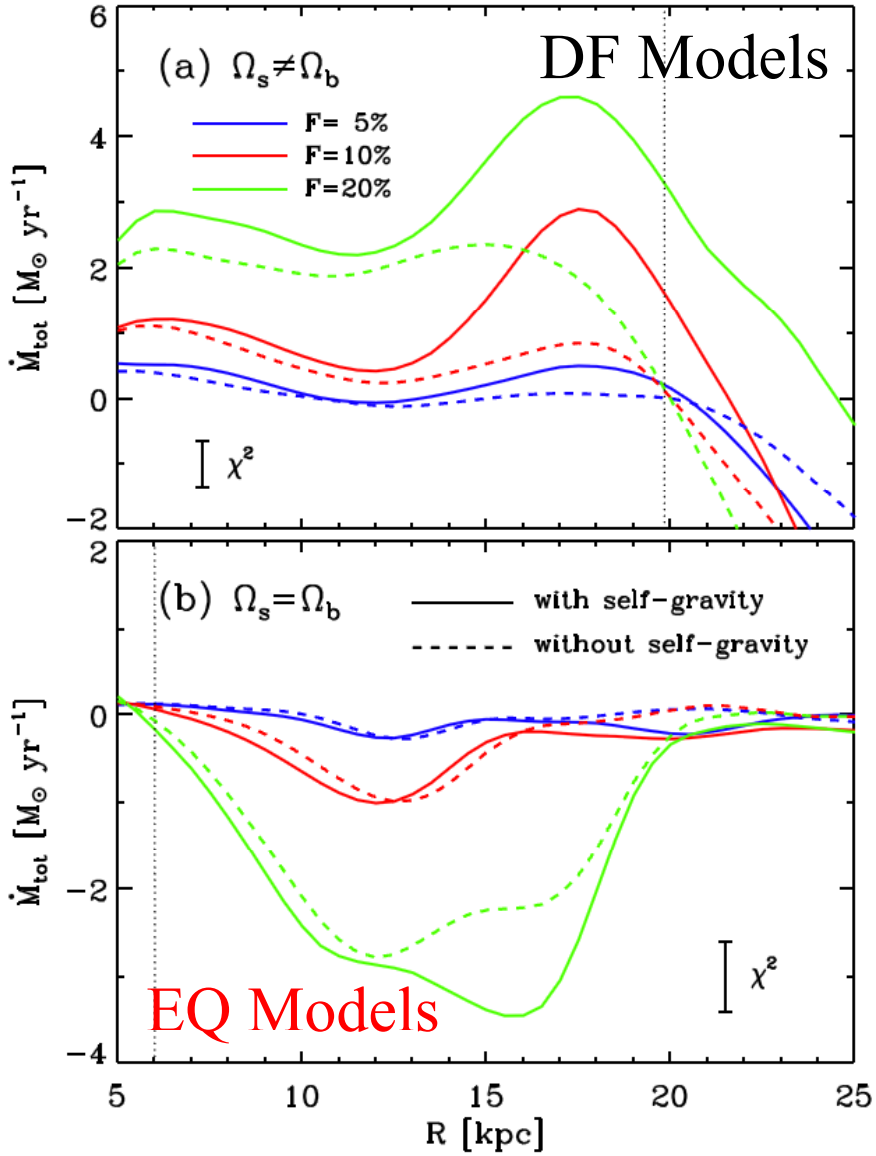

Mass Drift Rate

- The total rate of gas drift in our models is a combination of three processes:

$$\dot{M}_{\rm tot} = \dot{M}_{\rm shock} + \dot{M}_{\rm ext} + \dot{M}_{\rm self}$$

  - Dissipation of angular momentum at spiral shocks (Lubow et al. 1986; Hopkins & Quataert 2011)
  - Torque by the external spiral potential (Lubow et al. 1986)

$$\dot{M}_{\rm ext} = -\left(\frac{1}{R}\frac{\partial R^2\Omega}{\partial R}\right)^{-1}\int_{-\pi}^{\pi}\Sigma\frac{\partial\Phi_{\rm ext}}{\partial\phi}d\phi$$

  - Torque by the self-gravitational potential

$$\dot{M}_{\rm self} = -\left(\frac{1}{R}\frac{\partial R^2\Omega}{\partial R}\right)^{-1}\int_{-\pi}^{\pi}\Sigma\frac{\partial\Phi_{\rm gas}}{\partial\phi}d\phi$$

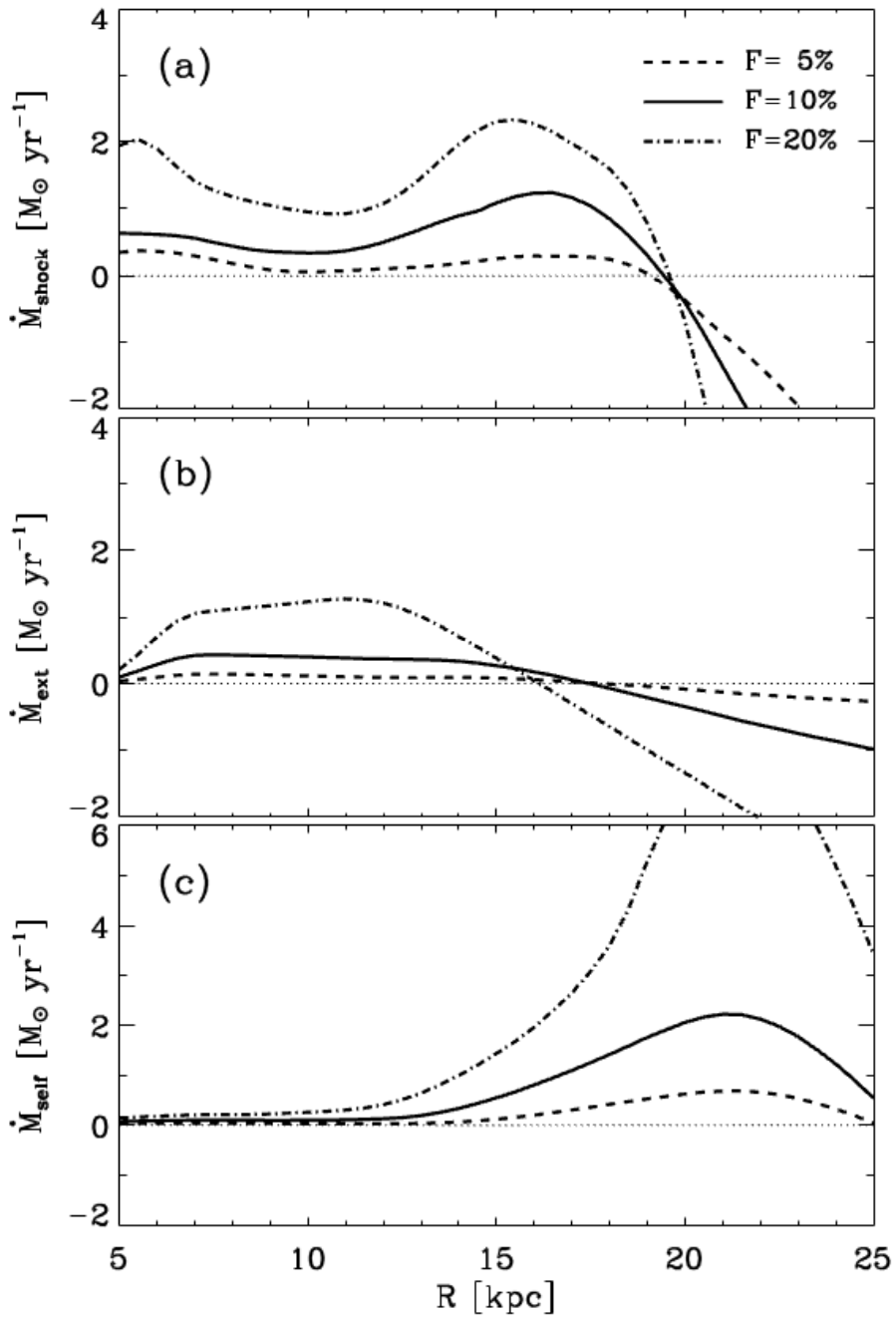

Mass Inflow Rate in DF models

- $\dot{M}_{\rm shock} > 0$ inside the CR, as expected.
- Shock: extG: selfG
  = 50% : 40%: 10%, on average.
- Total inflow rates:
  ~0.5–2.5$M_\odot$ yr^{-1} (for $\mathcal{F}$=5-20%)

$$\dot{M}_{\rm tot} = 8\mathcal{F}(1+\ 3\mathcal{F})\frac{\Sigma}{\Sigma_0} M_\odot \ {\rm yr}^{-1}$$

cf. Lubow et al. (1986)'s local models yield
$dM/dt \sim$ 0.2–0.4$M_\odot$ yr^{-1}
corresponding to $\mathcal{F}$=3%.

Gravitational Torque Analysis

NGC4579 from HI gas obs.
(García-Burillo et al. 2009)

$$t(R) = \frac{\int_\theta N(x,y) \times (x\,F_y - y\,F_x)}{\int_\theta N(x,y)}$$

$$\frac{\Delta L}{L} = \frac{\mathrm{d}L}{\mathrm{d}t}\bigg|_\theta \times \frac{1}{L}\bigg|_\theta \times T_{\rm rot} = \frac{t(R)}{L_\theta} \times T_{\rm rot}$$

$$\frac{\mathrm{d}^2 M}{\mathrm{d}R\mathrm{d}t} = \frac{\mathrm{d}L}{\mathrm{d}t}\bigg|_\theta \times \frac{1}{L}\bigg|_\theta \times 2\pi R \times N(x,y)|_\theta$$

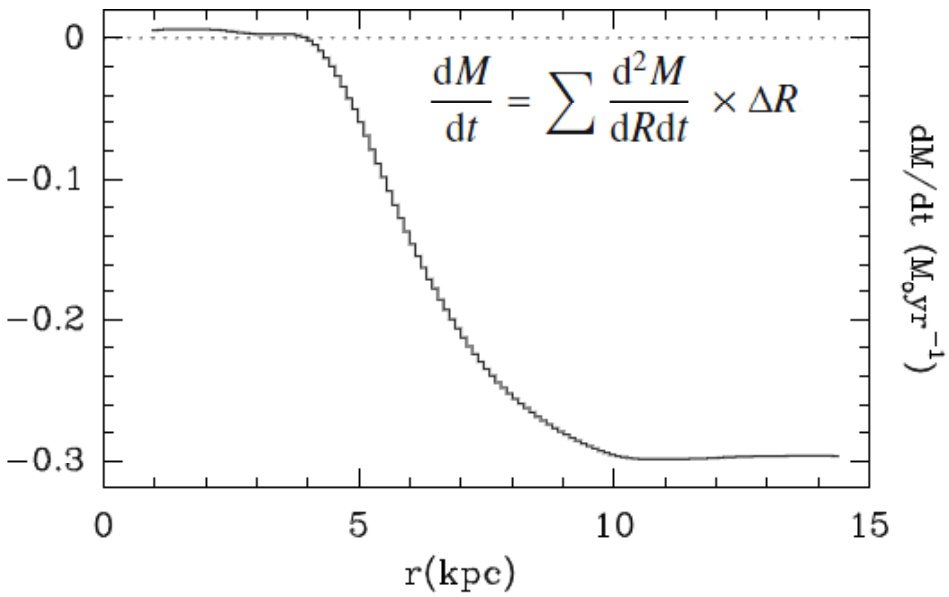

Haan et al. (2009)

Table 9
Gravitational Torque Analysis

Source	$\langle dL/L \rangle$		$\langle \lvert dL/L \rvert \rangle$		$dM_{\rm HI}/dt$	$dM_{\rm mol}/dt$	$R_{\rm max,HI}$	$R_{\rm max,CO}$
	H I	CO	H I	CO	($M_\odot$ yr^{-1})	($M_\odot$ yr^{-1})	(kpc)	(kpc)
NGC 3368	0.02	−0.50	0.12	0.55	0.04	−11.11	13.0	0.35
NGC 3627	−0.00	0.16	0.26	0.24	−0.10	50.13	6.0	0.75
NGC 4321	0.01	0.02	0.10	0.10	−0.18	1.03	18.0	1.2
NGC 4736	0.02	0.01	0.03	0.09	0.06	−0.01	8.5	0.62
NGC 5248	0.06	−0.02	0.13	0.02	0.49	−22.96	20.5	0.8
NGC 6951	−0.04	−0.05	0.09	0.10	−0.16	−4.29	29.0	1.0
NGC 7217	−0.01	−0.02	0.03	0.03	−0.01	−2.37	15.2	1.4

Inner Ring Mass

- The inflowing gas due to spiral arms in the DF models can move across the outermost x_1-orbit and secularly increases the gas mass in the bar region.

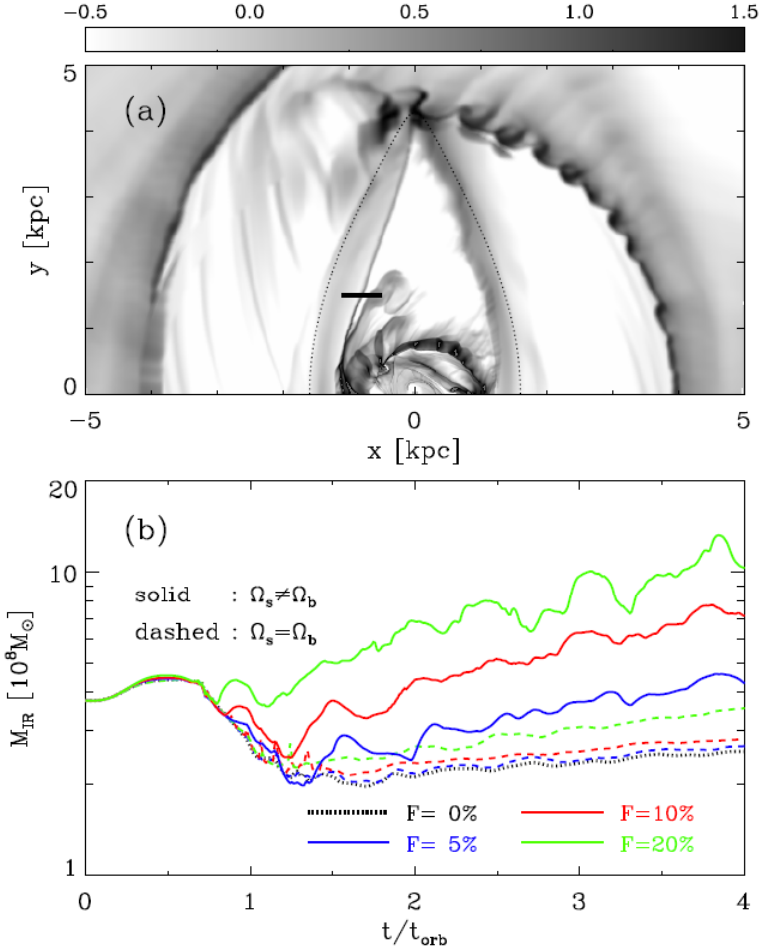

- About 15% of the total inflowing gas encircles the bar region outside the outermost x_1-orbit.
- About 60% is used to increase the gas mass in the inner ring.

Dust Lane Strength

- About 5% of the inflowing gas goes to the dust lanes.
- For $\mathcal{F}$=10%, dust lanes can be readily visible for a long period of time against background stellar radiation.

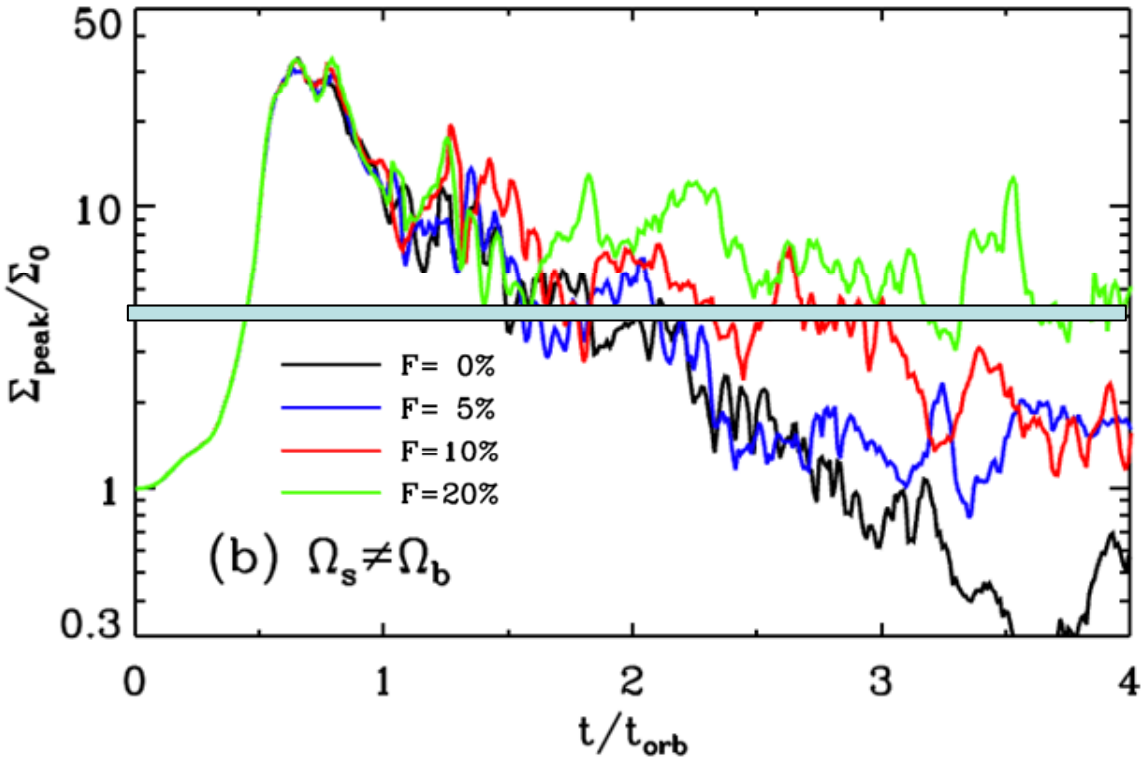

A_V=3 for Σ_0=10 $M_\odot$ pc^{-2}

Nuclear Ring Mass

- About 20% (~0.3 $M_\odot$ yr^{-1} when $\mathcal{F}$=10%) of the inflowing gas goes to the nuclear ring.

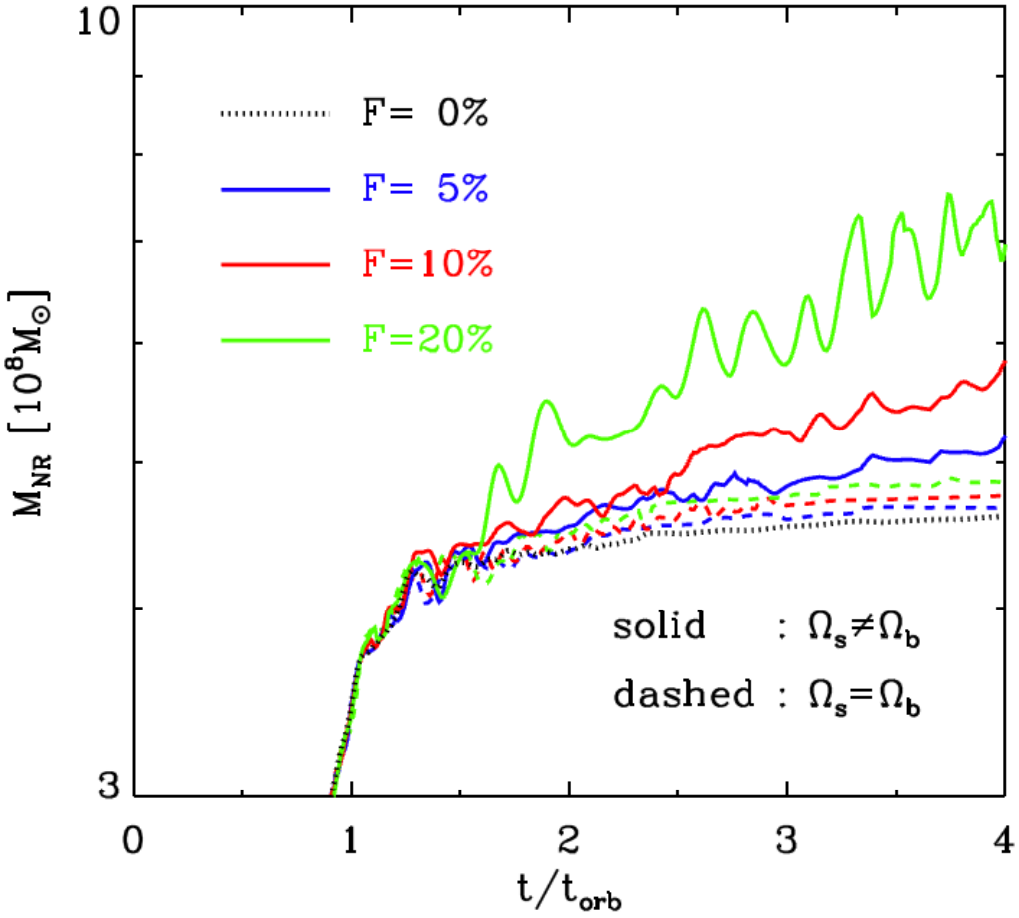

Kinematic Differences in DF and EQ models

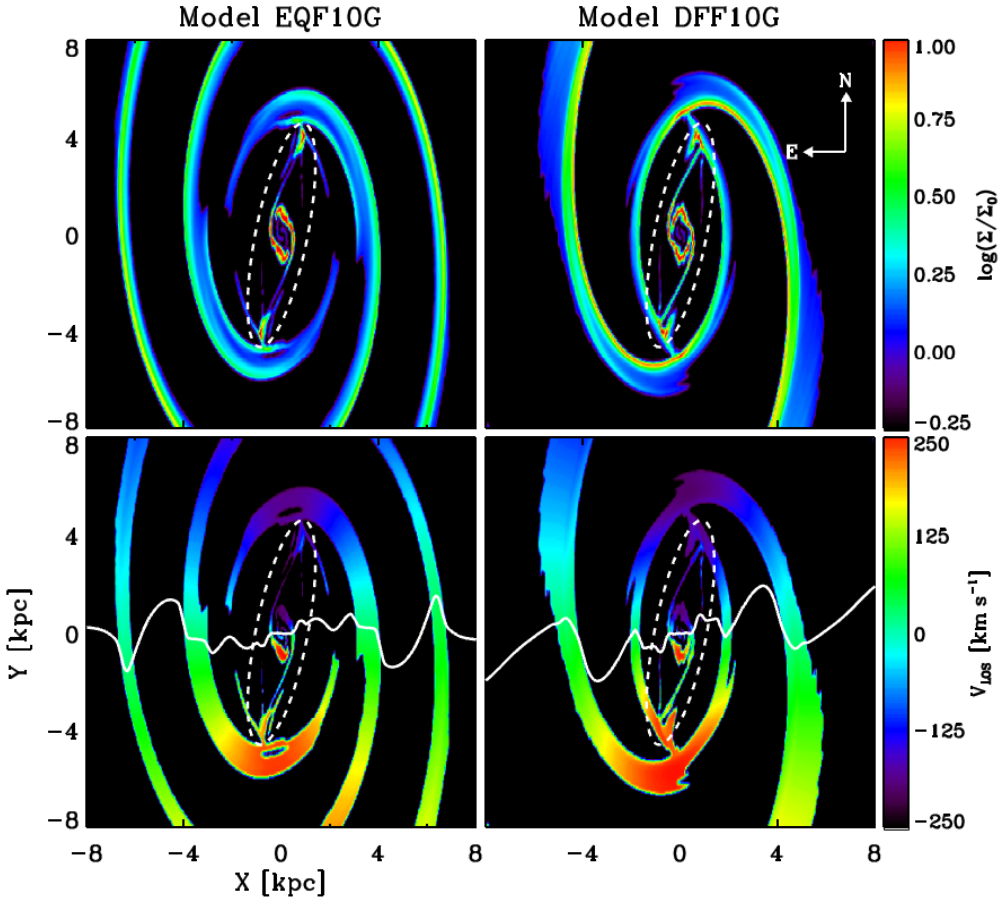

Regan et al. (2002)

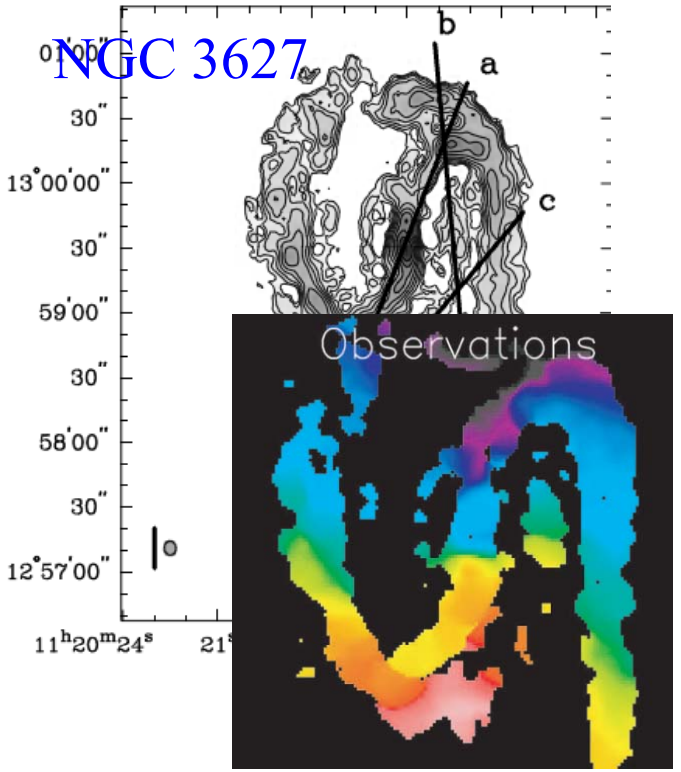

Ω_b= 50 km s^{-1} kpc^{-1}
Ω_s= 23 km s^{-1} kpc^{-1}
(Rand & Wallin 2004)

- Gaseous arms are more loosely wound in DF models.
- The arms have larger density at smaller *R* in DF models.
- Due to streaming motions, the zero velocity curve near the western (eastern) arms strongly bends downward (upward) in DF models.

Summary

- Bar Regions
  - Gaseous bar substructures readily form via interaction with a non-axisymmetric bar potential.
  - Dust lanes are more straight in more strongly barred galaxies
  - Nuclear rings form not by resonances but by the centrifugal barrier that the inflowing gas cannot overcome.
- Spiral-arm regions
  - Spiral arms are efficient to drive radial mass inflows at the level ~0.5–2.5$M_{\odot}$ yr^{-1} , provided the arm pattern speed is much smaller than that of the bar, enhancing the strength of bar substructures.
  - The extent of spiral shocks is limited by too large $\mathcal{M}_{\perp}$ in EQ models.
  - The arm pitch angle of gaseous arms is in general smaller than that of the stellar arms.